AD-A145 987 GYROTRON BEAM GENERATION WITH HELICAL MAGNETIC FIELDS 1/1
(U) MISSION RESEARCH CORP ALEXANDRIA VA
R H JACKSON ET AL. AUG 83 MRC/WDC-R-061
UNCLASSIFIED N00014-82-C-2206 F/G 20/7 NL

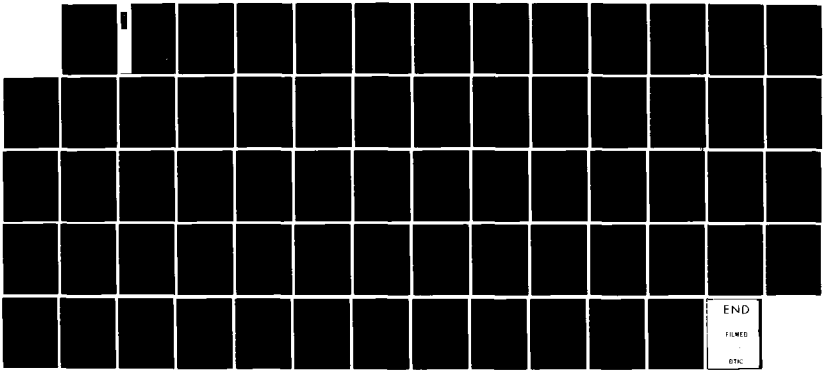

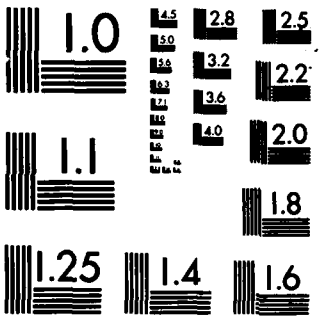

MRC/WDC-R-061

FINAL REPORT

GYROTRON BEAM GENERATION WITH HELICAL MAGNETIC FIELDS

R. H. Jackson
C. A. Sedlak

August 1983

Prepared for: Naval Research Laboratory
Code 6840
4555 Overlook Avenue, S.W.
Washington, DC 20375

Contract No. N00014-82-C-2206

MISSION RESEARCH CORPORATION
5503 Cherokee Avenue, Suite 201
Alexandria, Virginia 22312
(703) 750-3556

Copy 19

MRC/WDC-R-061

FINAL REPORT

GYROTRON BEAM GENERATION WITH HELICAL MAGNETIC FIELDS

R. H. Jackson
C. A. Sedlak

August 1983

Prepared for: Naval Research Laboratory
Code 6840
4555 Overlook Avenue, S.W.
Washington, DC 20375

Contract No. N00014-82-C-2206

MISSION RESEARCH CORPORATION
5503 Cherokee Avenue, Suite 201
Alexandria, Virginia 22312
(703) 750-3556

ABSTRACT

This report presents the results of an investigation into the basic properties of a new type of electron gun for generating high transverse velocity beams, the bifilar helix - Pierce gun or H-gun. The H-gun differs significantly from presently used magnetron injection guns (MIGs) in that first a laminar, low transverse velocity beam is formed and then transverse velocity is imparted by propagating the beam through the magnetic field of a bifilar helix. In order to evaluate the H-gun, an analytic and computational study was conducted to examine the relationships between the magnetic fields (axial and helical), and the beam properties after exiting the helical field. The effects of the helix field entrance profile, the helix-axial field gyroresonance, and helix field gradients have been taken into account in the investigation. Based on the results of this research, conditions have been specified which will produce a high transverse velocity beam with low axial velocity spread. In particular, it has been found that an adiabatic helix entrance profile can provide a flexible means of generating high quality beams for gyro-devices.

CONTENTS

LIST OF FIGURES & TABLES

LIST OF FIGURES & TABLES (Continued)

FIGURES PAGE

TABLES

LIST OF SYMBOLS
(cgs units are used unless otherwise indicated)

c	speed of light in vacuum
e	magnitude of electron charge
m	electron rest mass
β_i $(= v_i/c)$	normalized velocity
β_o	magnitude of total velocity
$\gamma(=(1-\beta_o^2)^{-1/2})$	relativistic mass factor
$\beta\perp$	magnitude of transverse velocity for an ideal orbit in axial and ideal helical magnetic fields
β_{zo}	axial velocity of ideal orbit
$\alpha(=\beta\perp/\beta_{zo})$	velocity ratio
$A(=1-(1+\alpha^2)^{-1/2})$	constant used in normalized orbit equations
δ, δ_z	transverse and axial velocity perturbations of the ideal orbits
$r\perp$	radius of ideal orbit
δr	radial perturbation of ideal orbit
B_h	on-axis magnitude of helix field
B_z	axial guide field
B_T	transition axial magnetic field
ω_z, ω_h	cyclotron frequency of axial and helical magnetic fields
B_1	axial field in helix region
B_2	axial field in RF interaction region
$R(=B_1/B_2)$	magnetic compression ratio
η	normalized axial magnetic field strength

ν	normalized helix field strength
a	helix radius
L	helix period
k_w (= $2\pi/L$)	helix wavenumber
I_h	helix current
HC	helix cosine integral
HS	helix sine integral
ε (= $k_w a$)	normalized helix radius
ξ = ($k_w z$)	normalized axial distance
I_n, K_n	modified Bessel functions of the first and second kind
L_n	modified Struve function
K	complete elliptic integral of the first kind
'	denotes derivative with respect to the argument
•	denotes derivative with respect to time
σ ( ) Sigma ( )	denotes standard deviation
|...|	absolute value

SUMMARY

Growing interest in microwave devices utilizing the cyclotron maser instability has motivated investigation of improved techniques for generating the high transverse velocity electron beams required for efficient operation. One approach which has recently been suggested is to combine a confined-flow Pierce gun with the transverse magnetic field of a bifilar helix. The Pierce gun generates a high quality, low transverse velocity beam and the helical magnetic field deflects the beam developing the perpendicular velocity. The basic characteristics of this combination, called the helix gun or H-gun, have been studied analytically and computationally for two helix configurations. In one case the helix magnetic field gradually increases over several helix periods, adiabatic entrance, and in the other, the field is assumed to increase to full amplitude over a distance negligible compared to the helix period, nonadiabatic.

The relationship between the transverse beam velocity and the applied axial focusing and helical magnetic fields was explored analytically using the lowest order approximation to the helix field. A resonant enhancement of the helix field was found to occur when the axial cyclotron wavelength was approximately equal to the helix period. This resonance can be exploited to reduce greatly the helix field needed to achieve a given transverse velocity. For cyclotron wavelengths close to but longer than the helix period, the electron orbits are found to be unstable to perturbations. Expressions have been derived to relate the transverse velocity to the fields for the adiabatic and nonadiabatic cases. By normalizing the magnetic fields, curves which are valid for all H-guns can be drawn relating the field magnitudes and velocity.

To examine the effects of the helical field on beam velocity spread, improved models of the helix field are needed. Expressions for the off-axis fields of an infinite bifilar helix were found in the

literature. These formulas were extended to include multiple wire coils and corrections to the fields for the adiabatic entrance case. Equations were also derived for the on-axis fields of a semi-infinite nonadiabatic helix. The more accurate field expressions are complex enough that general analytic work is not possible.

The improved field models were included in a trajectory code and the beam characteristics at the helix exit were investigated computationally. The agreement between the analytic results and the computations was reasonable, especially for the nonadiabatic entrance case. For both helix types the beam velocity spread was found to increase as the resonance was approached. The unstable region where the cyclotron wavelength is longer than the helix period was found to generate substantially higher velocity spreads than other regions. The adiabatic entrance was found to generate slightly higher quality beams than the nonadiabatic entrance.

The computational results indicate that beams with velocity ratios, $\alpha = \beta_\perp / \beta_z$, of approximately 1 at the exit of the helix can be generated with less than 2% axial velocity spread. This level of performance would certainly make the H-gun competitive with the magnetron injection gun. The slightly higher beam quality and greater flexibility of the adiabatic helix suggest that it should be the preferred configuration for resarch and proof-of-principle experiments. In situations where ease of fabrication, compactness, or efficiency are most important a nonadiabatic helix is more appropriate.

Future research on H-guns should include important beam effects, such as self fields and improved models of the helix field. In addition, H-gun related configurations using hollow beams and/or different types of transverse magnetic fields should be investigated.

SECTION 1
INTRODUCTION

One source of problems in the design and operation of gyro-devices is the magnetron-injection gun (MIG) which produces the high transverse velocity electron beam. MIGs operate with crossed electric and magnetic fields so that the electron beam is formed and given large transverse velocities at the same time. Because beam formation and production of transverse velocity are combined, MIGs are fairly inflexible. Changes in voltage or magnetic field generally require a new design. (MIGs do not scale as well as Pierce guns.) Even changes in the operating current can require design adjustments. Another problem is the high thermal spreads (several %) caused by temperature limited emission. Thermal velocity spreads can lower interaction efficiency and produce high noise levels (which affects amplifier operation). Additional problems include high cathode loading factors, and the inability to produce solid electron beams.

Several new gun configurations are presently under investigation to overcome the problems associated with the use of MIGs in gyro-devices. The helix gun (H-gun) is one approach being considered for use in Navy programs and has recently been used in a gyro-TWT experiment[1] with encouraging initial results. The H-gun completely separates beam formation from the problem of imparting large transverse velocities to the electrons. The gun used for beam formation can be any of several standard designs which produce beams with little or no perpendicular velocity (e.g. Pierce guns). Perpendicular beam velocity is produced by propagating the beam through the transverse magnetic field of a bifilar helical winding. The H-gun system has the potential of generating high quality beams (low axial velocity spreads) while permitting wide variation in magnetic fields and transverse velocity.

A schematic of a possible H-gun configuration is shown below in Figure 1-1. In this example a confined-flow Pierce gun generates a solid beam which is focused into a uniform axial and helical magnetic field. The helical field generates transverse velocity on the beam. The beam is then extracted from the helix and compressed into the interaction region. There are several advantages to this configuration. The electron gun can be operated space charge limited yielding a longer cathode life, grid control, and lower beam noise. The use of a confined flow laminar electron gun permits greater variation in beam voltage and magnetic field. Controlling the transverse velocity with the helix magnetic field gives an independent "knob" which can be used to tune the beam characteristics. In addition to these factors, H-gun designs are easily scaled to new parameter domains.

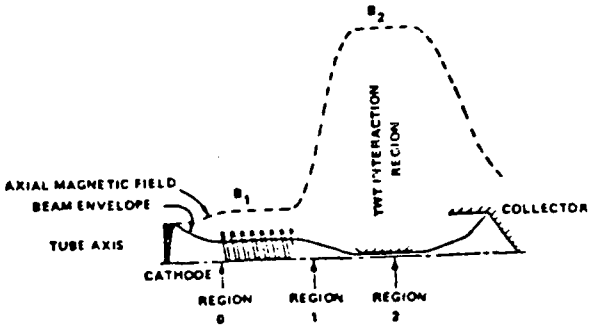

Figure 1-1. A possible H-gun configuration; region 0 is a confined-flow Pierce gun and bifilar helix, region 1 is the adiabatic magnetic compression, and region 2 is the RF interaction space.

The following sections of this report will discuss the effects of the helical field on the beam properties at the exit from the helix. The next section will discuss beam motion in a uniform axial and "ideal" helical magnetic field. The general properties of the beam motion and the relationship between the fields and the beam velocities will be described. Section 3 will discuss models of the helix field that are closer to what can be achieved in the laboratory and how these changes affect the beam properties. Section 4 will present the results of computer calculations of beam propagation in the combined fields with the more realistic helix models. H-gun design and scaling laws will be described in Section 5, and conclusions presented in Section 6.

Before proceeding to the technical discussion some general comments about this investigation and beam quality issues should be made. In order to concentrate on the effects of the helical field on the beam, space charge forces have been ignored. In addition, the electron beam is assumed to have no initial transverse velocity. The impact of these simplifications can not be ignored in the development of practical guns. One must emphasize that in order to extract a high quality beam from the helix, a high quality beam must be injected. Thus, beam quality in the H-gun must start with the Pierce gun design. If the gun is designed well and a laminar, low ripple beam is injected into the helix, then performance levels close to those discussed here should be achievable even with space charge effects.

The quality of the beam in the RF interaction section also depends on the magnetic compression between the helix and interaction regions. The adverse effects of the compression can be illustrated by referring to Figure 1-2. These curves relate the velocity ratio, $\alpha = \beta_\perp / \beta_z$, at the helix exit to the ratio in the interaction region through the compression ratio, R. Clearly, the compression magnifies any velocity spreads which exist at the helix exit. (This is a problem which also occurs in the MIG.) The H-gun configuration has the potential of eliminating this problem by generating the transverse velocity in an axial field of the same magnitude as the interaction field. In order to operate the H-gun in this mode one must be able to generate large helical fields. Under the appropriate circumstances helical fields of many kilogauss can be generated with either permanent magnets[2] or cryogenic bifilar helices[3]. Although these systems are not appropriate for experimental study of the H-gun, their potential must be kept in mind when considering H-gun designs for actual devices.

One further comment on the design of H-guns should be made. The results presented here should prove useful as a guide to selecting H-gun parameters and to scaling successful designs. However, there can be no

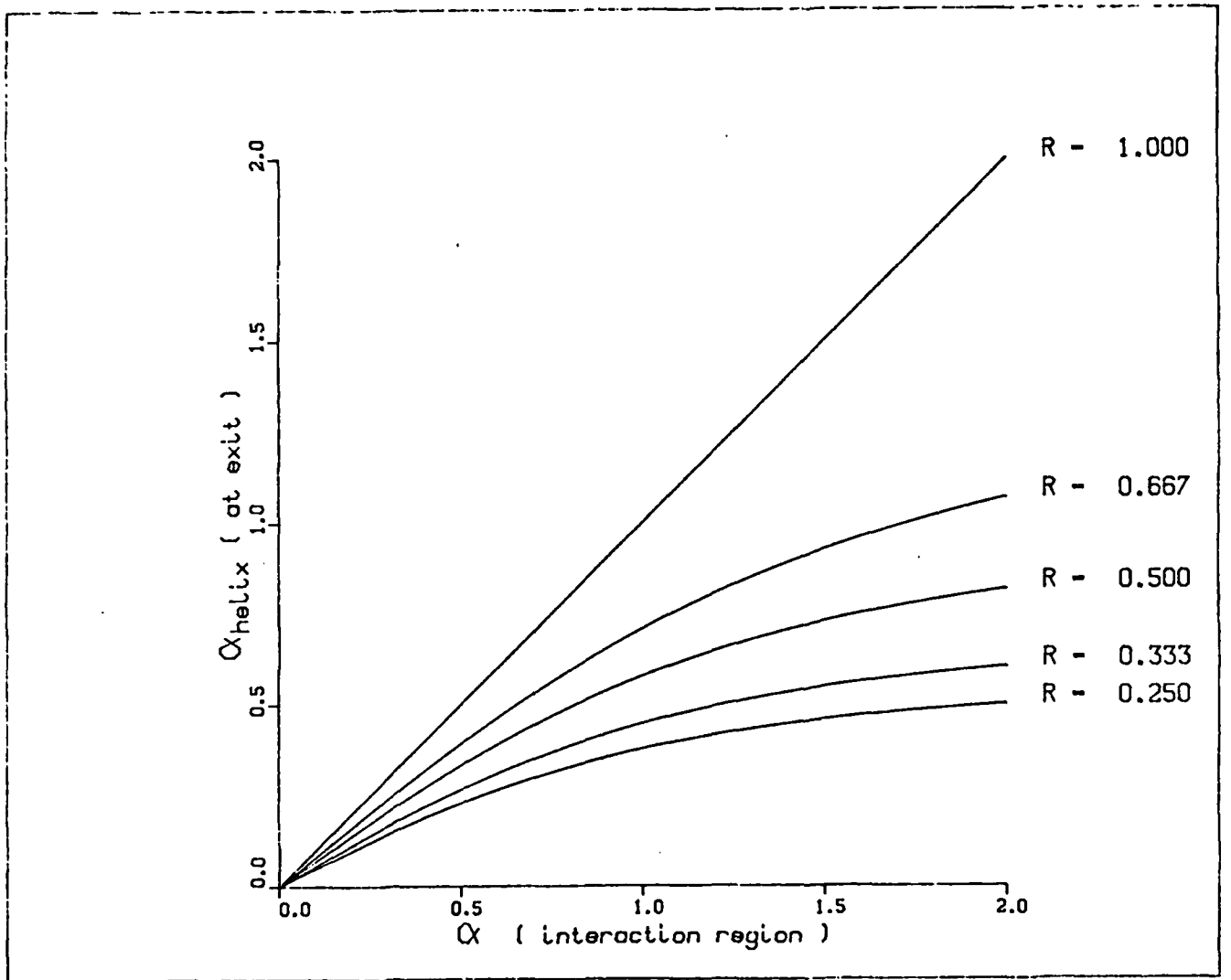

Figure 1-2. The velocity ratio ($\alpha = \beta_1/\beta_z$) at the helix exit necessary to produce a desired ratio in the interaction region as a function of magnetic compression ratio, $R = B_1/B_2$. Note that for the smaller Rs a small velocity spread at the helix exit produces a large spread after compression.

substitute for doing detailed calculations on the specific system to be used in an experiment including as many of the physically important effects as possible. This approach coupled with experimental diagnostics is presently the only method that will provide the detailed information necessary to validate the H-gun concept.

SECTION 2
IDEAL HELICAL FIELD H-GUNS

In this section the basic properties of beam motion in uniform axial and ideal helical fields will be developed. "Ideal" means that the field magnitude is constant and that the field orientation depends only on z. A coil that would produce a helical magnetic field is shown schematically in Figure 2-1. The magnetic field near the axis of such a coil closely approximates an ideal helical field. Over the past two decades a great deal of research has been published on electron orbits in these fields[4-10]. Exact solutions[6,10] can be obtained for the particle orbits, but the expressions are somewhat cumbersome and tend to distract one from the general physical features of the motion. Here, we will concentrate on two cases of particular interest to the H-gun, the limits of adiabatic and nonadiabatic increase of the helix field. Readers desiring more detailed information on the general orbits should consult References 4-10.

The combined magnetic fields are given by the equation

$$\underline{B} = B_h(\hat{e}_x \cos k_w z + \hat{e}_y \sin k_w z) + \hat{e}_z B_z$$

where $\hat{e}_i$ is a unit vector in the ith direction, B_h is the helix field magnitude, B_z is the axial field magnitude, $k_w = 2\pi/L$, and L = helical field period. Electron orbits in the field were studies using the above magnetic field in the Lorentz force and the relativistic Newton's equation. After some algebra the equations of motion can be written as

$$\dot{\beta}_x = \beta_z \omega_h \sin k_w z - \omega_z \beta_y$$

$$\dot{\beta}_y = \omega_z \beta_x - \omega_h \beta_z \cos k_w z \qquad (1)$$

$$\dot{\beta}_z = \omega_h (\beta_y \cos k_w z - \beta_x \sin k_w z)$$

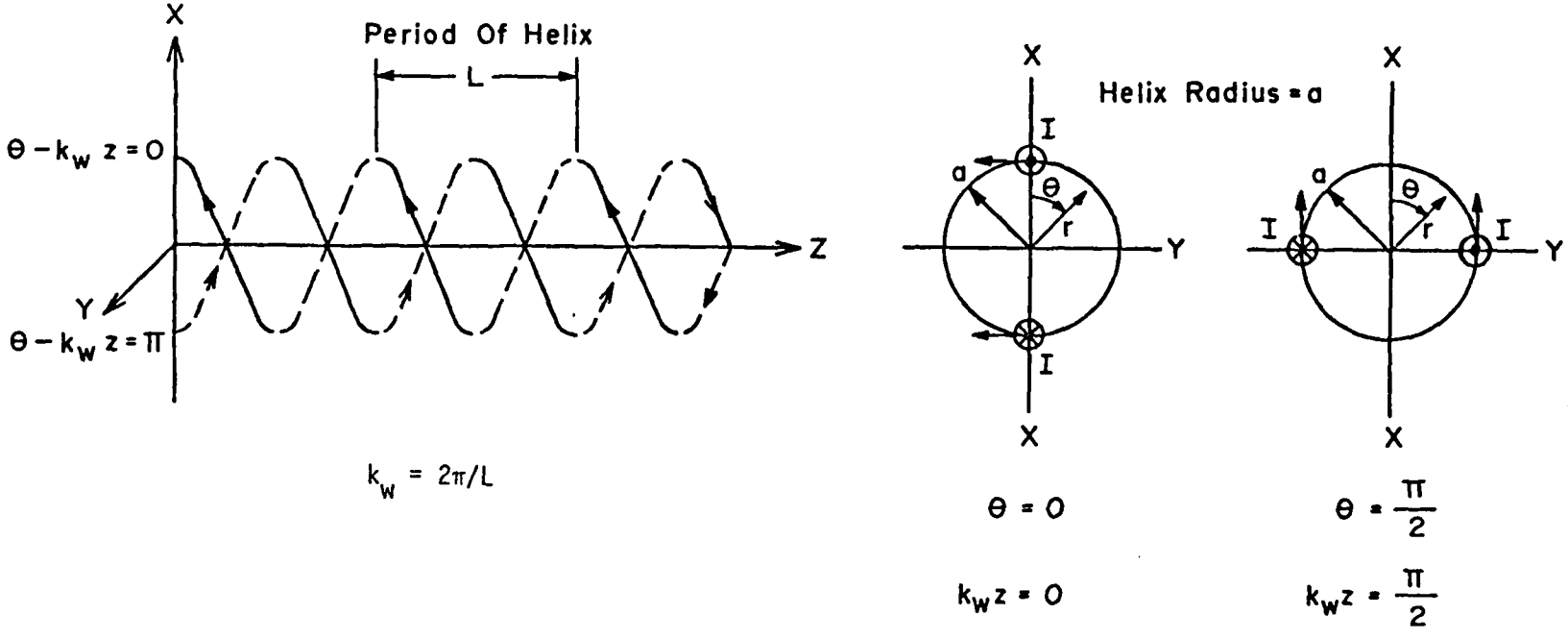

Figure 2-1 Geometry and characteristics of a right-hand circularly-polarized bifilar helix which is typically used to generate transverse helical fields.

where $\beta_i = v_i/c$, c = speed of light in vacuum, $\omega_{h,z} = eB_{h,z}/mc\gamma$, are the helix and axial magnetic field cyclotron frequencies, and $\dot{}$ stands for differentiation with respect to time. There are two constants of the motion which can be derived from these equations. The first is conservation of energy and is easy to derive. The second is somewhat more complex and depends on the simplified form that has been chosen for the helical magnetic field. These constants are given by

$$\beta_o^2 = \beta_x^2 + \beta_y^2 + \beta_z^2 \tag{2}$$

$$C_o = \beta_x \cos k_w z + \beta_y \sin k_w z - \frac{ck_w}{2\omega_h}\left(\beta_z - \frac{\omega_z}{ck_w}\right)^2 . \tag{3}$$

These constants along with equations (1) can be solved to give the exact orbits[6,10] for arbitrary initial conditions. The two cases chosen for investigation here do not require the full power of this approach, so at this point we will tailor the equations to the examples.

The adiabatic helix will be considered first. In an adiabatic helix the field magnitude is gradually increased in an attempt to place the electrons on constant axial velocity orbits. Taking the second time derivative of the x and y velocity components in (1) gives

$$\begin{aligned} \ddot{\beta}_x + \omega_z^2\beta_x &= \omega_h\beta_z(\omega_z + c\beta_z k_w)\cos k_w z + \omega_h\dot{\beta}_z \sin k_w z \\ \ddot{\beta}_y + \omega_z^2\beta_y &= \omega_h\beta_z(\omega_z + c\beta_z k_w)\sin k_w z - \omega_h\dot{\beta}_z \cos k_w z . \end{aligned} \tag{4}$$

If the field entrance is adiabatic enough, then the $\dot{\beta}_z$ terms in (4) can be set equal to zero in the uniform helix field section. This leaves the well known equation for a harmonic oscillator with a forcing function. The particular solution is the one of principal interest; however, the

homogeneous solution will be included as a perturbation. The approximate solution to these equations is shown below.

$$\beta_x \simeq \beta_\perp \cos k_w z + \delta \cos(\omega_z t + Q)$$

$$\beta_y \simeq \beta_\perp \sin k_w z + \delta \sin(\omega_z t + Q)$$

$$\beta_z \simeq \beta_{zo} - \delta_z \cos(\omega_z t - k_w z + Q) \qquad (5)$$

$$x \simeq r_\perp \sin k_w z + \delta r \sin(\omega_z t + Q)$$

$$y \simeq -r_\perp \cos k_w z - \delta r \cos(\omega_z t + Q)$$

where

$$\beta_\perp = \frac{\omega_h \beta_{zo}}{\omega_z - ck_w\beta_{zo}}$$

$$r_\perp = \alpha/k_w,\ \alpha = \beta_\perp/\beta_{zo},\ \delta r = c\delta/\omega_z$$

$$\beta_{zo} = (\beta_o^2 - \beta_\perp^2)^{1/2},\ \beta_o = \text{total velocity/c}$$

$$\delta_z = \frac{\omega_h \delta}{\omega_z - ck_w\beta_{zo}},\ \text{and Q is a phase constant.}$$

This solution assumes that the z axis is the guiding center of the orbit, and that the following order holds

$$|\delta|,\ |\delta_z| \ll |\beta_\perp| < |\beta_{zo}|$$

and

$$r_\perp \ll a < L.$$

Although based on a simple model, there are several general features of the motion expressed by the above equations which will be found to carry over into more complex approximations to the H-gun.

The electron orbits are helical with the same basic period as the helical magnetic field. Small perturbations, due to the entrance and other factors, cause oscillations at the cyclotron frequency of the axial guide field and at the beat or difference frequency between the helix and guide cyclotron frequencies. One important characteristic is the gyroresonance which occurs when the cyclotron wavelength is approximately equal to the helix period. This leads to the resonant denominator ($\omega_z - ck_w\beta_{zo}$). The gyroresonance enhances the magnitude of the helix field and thereby increases the transverse velocity produced by a given helix amplitude. Note that the effects of perturbations on δ_z are enhanced, and that the axial velocity perturbation has a period which depends on the proximity of the guide field to gyroresonance. An effect which becomes important when devices and realistic fields are considered is the shift of the beam centroid off-axis. The beam center is shifted by an amount which depends on the helix period and the velocity ratio. For large velocity ratios the shift off-axis can be considerable. Note that the radial shift due to the perturbations has an absolute dependence on the guide field, being smaller the higher the field.

In order to solve for the quantities in these equations, conservation of energy must be used, eq. 2. This leads to a fourth order equation in the axial velocity. The orbits split into two types which are determined by whether the axial field is above or below the gyroresonance, i.e., $\omega_z > ck_w\beta_{zo}$, type II, or $< ck_w\beta_{zo}$, type I. Examination of perturbations of these orbits shows that the type I orbits become unstable[8] at

$$\omega_z = ck_w\beta_o(1 + \alpha^2)^{-3/2} ,$$

and remain unstable until $\omega_z > ck_w\beta_o(1+\alpha^2)^{-1/2}$. The instability occurs because of the gyroresonant denominator. If a perturbation decreases the axial velocity, then, for type I orbits, this decreases the resonant field and increases $\beta_\perp$ which further decreases β_z and so on. This instability can result in loss of the beam to the drift tube wall.

There are several ways of tapering the helix entrance field to obtain an adiabatic transition: the helix radius can be tapered, the current can be gradually decreased, the helix period can be decreased, the wires can be transitioned from bifilar to quadrafilar to bifilar with currents that cancel, etc. An example of an adiabatic transition that was achieved by tapering the helix radius[11] is shown in Figure 2-2. The effect that field tapering has on accessing constant velocity orbits is illustrated in Figure 2-3 where two orbits have been followed[12,13] computationally through the taper and into a uniform radius helix. The transverse velocity builds up slowly in the taper region and then oscillates in the uniform section. The average values of the velocities in the uniform section are in good agreement with ideal orbit calculations. The periods of the oscillations are in excellent agreement with the ideal orbit formula. The orbit represented by the solid line is closer to the gyroresonance. Hence, according to the ideal orbit equations (5), this orbit should have a larger and longer period perturbation than the orbit which is further from resonance. As can be seen in the figure, this is indeed the case.

In designing gyro-devices one is usually interested in achieving a particular velocity ratio, α. The orbit equation can be arranged to relate α, the helix field, and the guide field. Further, this equation can be normalized to take into account the beam voltage and helix parameters. First we will define the transition axial magnetic field

$$B_T = \frac{mc^2}{e}\beta_o\gamma k_w \qquad (6)$$

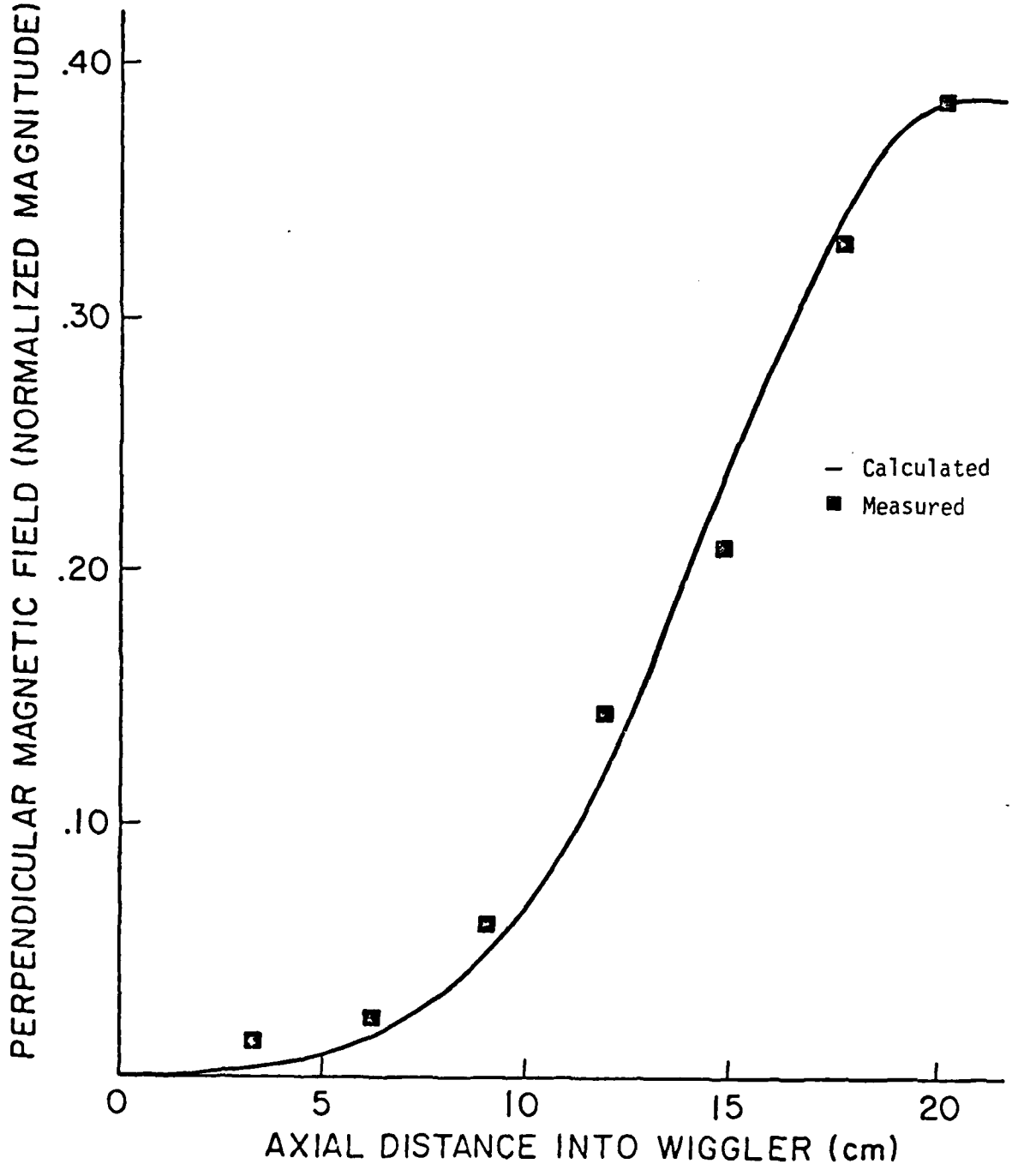

Figure 2-2 An adiabatic helix field increase obtained by starting the coils at a large radius and tapering down over seven periods (L=3 cm) to a smaller uniform radius. (See Ref. 11)

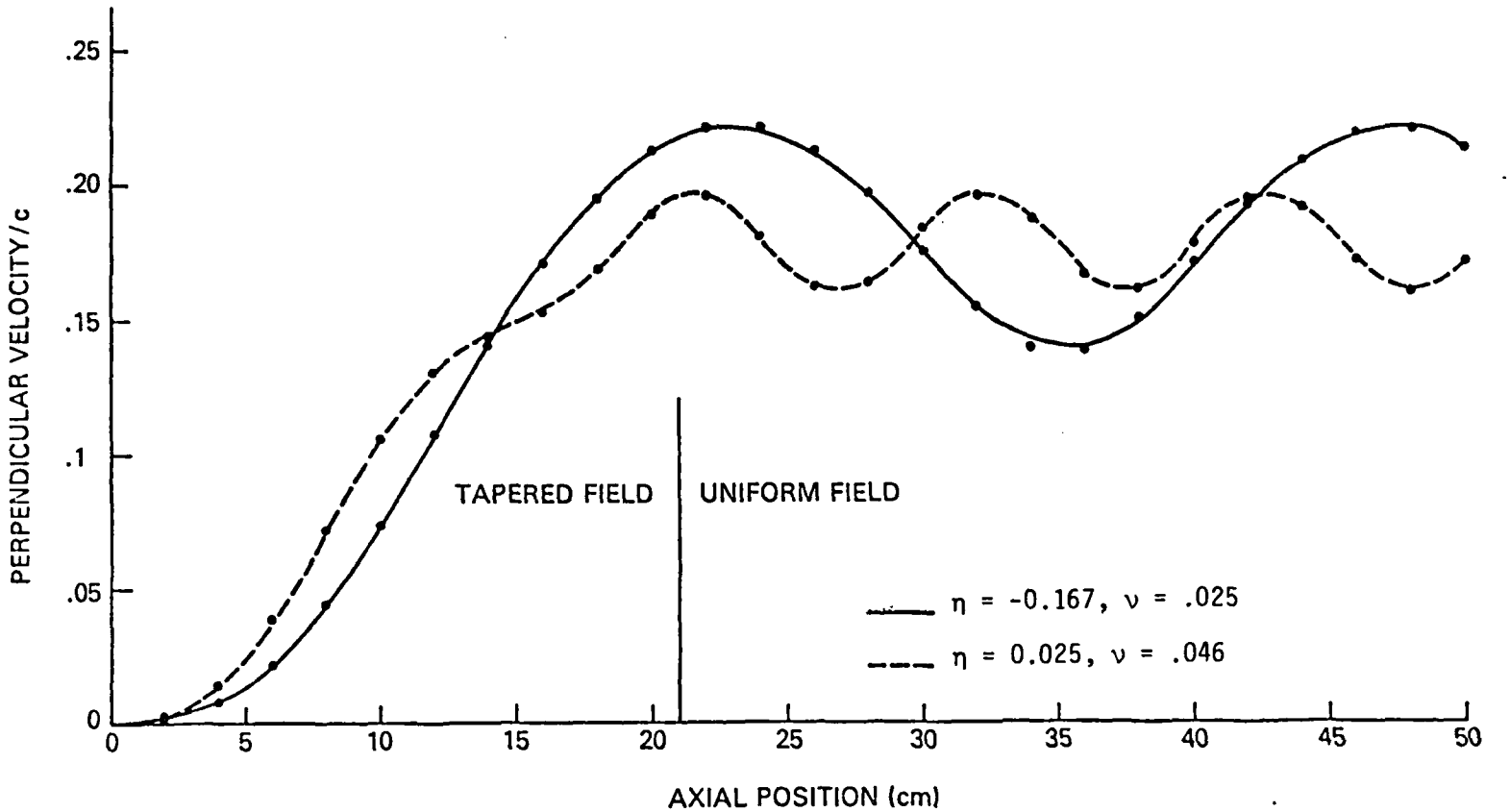

Figure 2-3 Evolution of the transverse velocity in the adiabatic helix field of Figure 2-2. The solid curve is for a type I orbit and the dashed curve for type II.

This parameter takes into account the helix period and beam voltage. By referring to the resonant denominator of Equation (5), one can see that B_T is also the highest magnetic field for which it is possible to drive the denominator to zero. Another way to state this is that for $B_z > B_T$ beam propagation is stable. Now B_T can be used to normalize the helix and guide fields:

$$\nu = B_h/B_T = \text{relative helix magnitude}$$

$$\eta = (B_z - B_T)/B_T = \text{guide field relative to gyroresonance.}$$

Using ν and η in the expression for $\beta_\perp$ gives

$$\alpha = \frac{\nu}{1+\eta - \beta_z/\beta_o} . \qquad (7)$$

Applying conservation of energy gives

$$\beta_z/\beta_o = (1 + \alpha^2)^{-1/2}$$

and

$$\nu = \left| \alpha (\eta + A) \right| \qquad (8)$$

where

$$A = 1 - (1 + \alpha^2)^{-1/2} .$$

Given α, Eq. (8) defines two straight lines (depending on the sign of α) which relate the normalized fields needed to produce that α. A set of α curves can be drawn which are valid for all H-gun designs. A set of these curves for several values of α are shown in Figure 2-4. Note that for $\eta < 0$ the lines cross each other and α becomes a multi-valued function of the fields. This is the region that will not support stable ideal orbits. One should also note that away from the resonance at $\eta < 0$, the helix

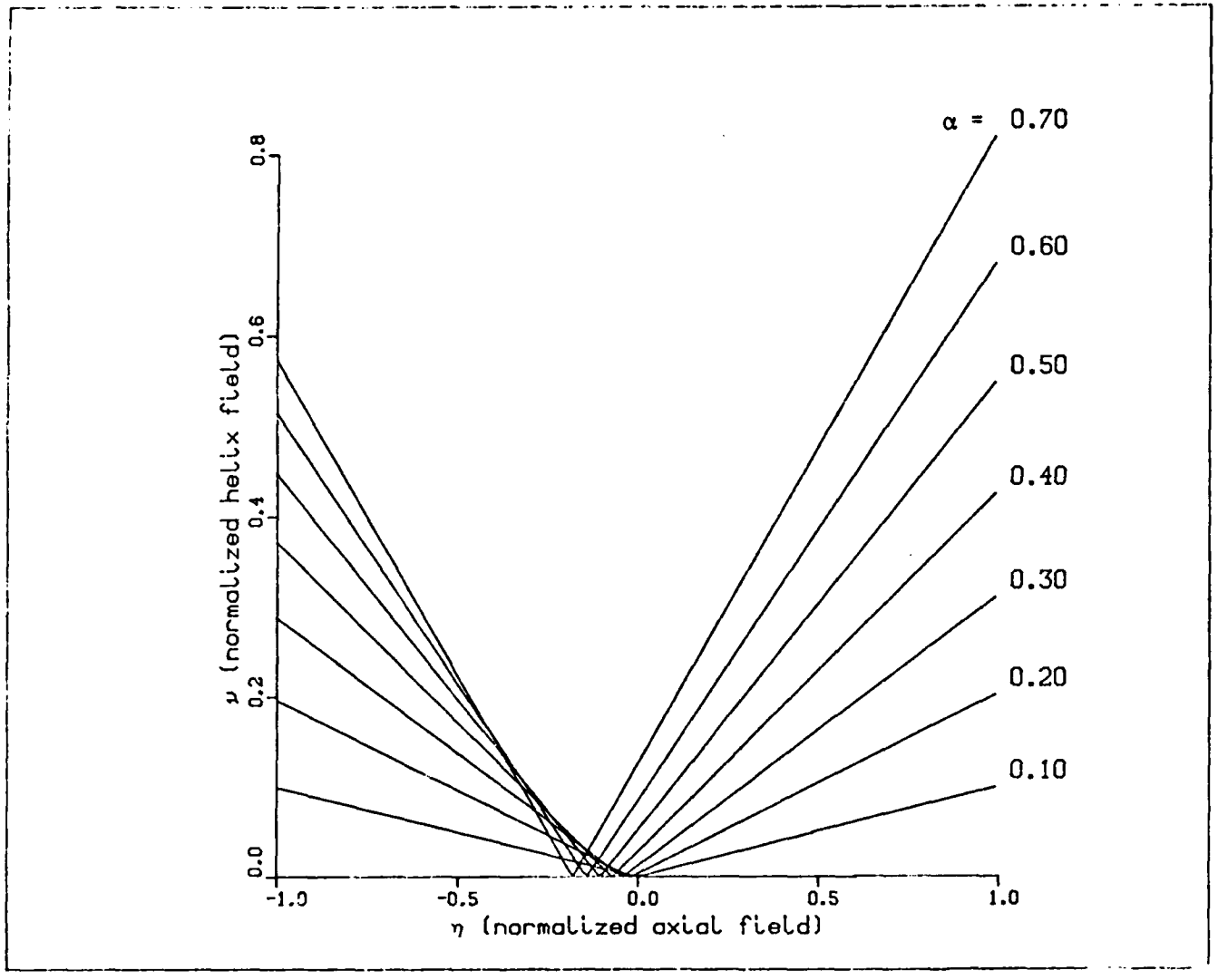

Figure 2-4 Scaling of fields and velocity ratio in an adiabatic helix. The fields are normalized using the transition magnetic field, Eq. 6.

field required to produce reasonably large α's becomes a sizable fraction of the guide field. For any set of ν, η, and α values there are many H-gun designs possible since the voltage, helix period, and real field strengths permit variations.

A similar analysis can be performed on a nonadiabatic helix. In this configuration the helix field rises very sharply to its final level. For analytic convenience we will assume that the field rises instantly to a constant magnitude. The orbit of an electron which enters this field with no transverse velocity is not a uniform velocity orbit. Instead the particle velocity will oscillate from $\alpha = 0$ to $\alpha = \alpha_{max}$. The helix field and particle orbit are illustrated in Figure 2-5 below. We will assume that the beam is extracted at the first position where $\alpha = \alpha_{max}$. For H-gun design purposes we need to find a relation between the fields and α, and a relation between these factors and the axial position at which α_{max} occurs.

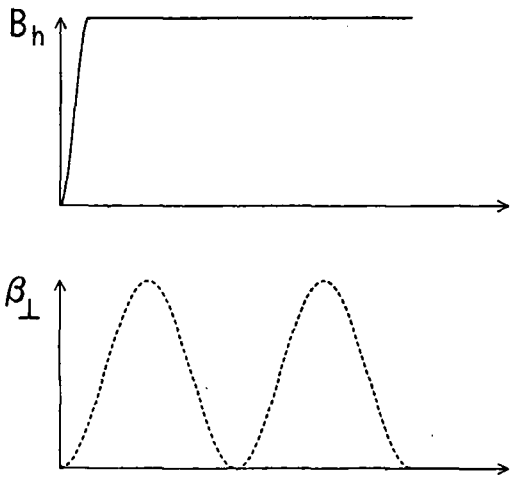

Figure 2-5 Illustration of the field profile and orbits in a nonadiabatic helix entrance.

The equations of motion are more complex for the nonadiabatic helix; however, using the normalized fields and the constants of motion α_{max}, ν, and η can be related. Starting with the $\dot{\beta}_z$ equation in (1), squaring, using the constants of motion assuming no initial transverse velocity, an elliptic integral solution for β_z can be found. If only the maximum α is needed, then the $\dot{\beta}_z$ term is zero and discarding the $\alpha = 0$ solution, the following cubic is obtained

$$4A\eta^2 + 4A^2\eta + A^3 + 4A\nu^2 - 8\nu^2 = 0$$

where A, η, ν are the same as for the adiabatic case. For particular A's, i.e. α's, this equation can be solved to relate the normalized fields,

$$\nu = \sqrt{\frac{A}{2 - A}} \left|\eta + A/2\right| . \qquad (9)$$

This equation is similar to Eq. (8) with a different slope and intercept on the η axis. A set of α curves for the nonadiabatic helix is shown in Figure 2-6. As in the adiabatic case, there is a region where α has a multi-valued dependence on the fields. As will be shown in Section 4, the region is "unstable" in that the beam is sensitive to small perturbations. Comparing these curves with those shown in Figure 2-6, note the lower helix field needed to achieve the same α. The trade-offs involved in selecting which helix entrance to use will be discussed later.

Equation 9 can also be solved for α_{max} given ν and η. This involves solving a cubic equation for A which can be done by standard means[14]. The final item needed for a preliminary nonadiabatic helix design is the axial position at which the first α_{max} occurs. This can be obained from the elliptic integral expression for β_z and is shown below for the case $\eta + A/2 > 0$,

$$Z = k_w z = 2\,(pq)^{-1/2}\left[2K(\mu) - \frac{1}{\mu}\,\ln\left(\frac{\sqrt{1-\mu^2}\,A^2 - \mu\sqrt{1-A^2}}{1 - \mu}\right)\right]. \qquad (10)$$

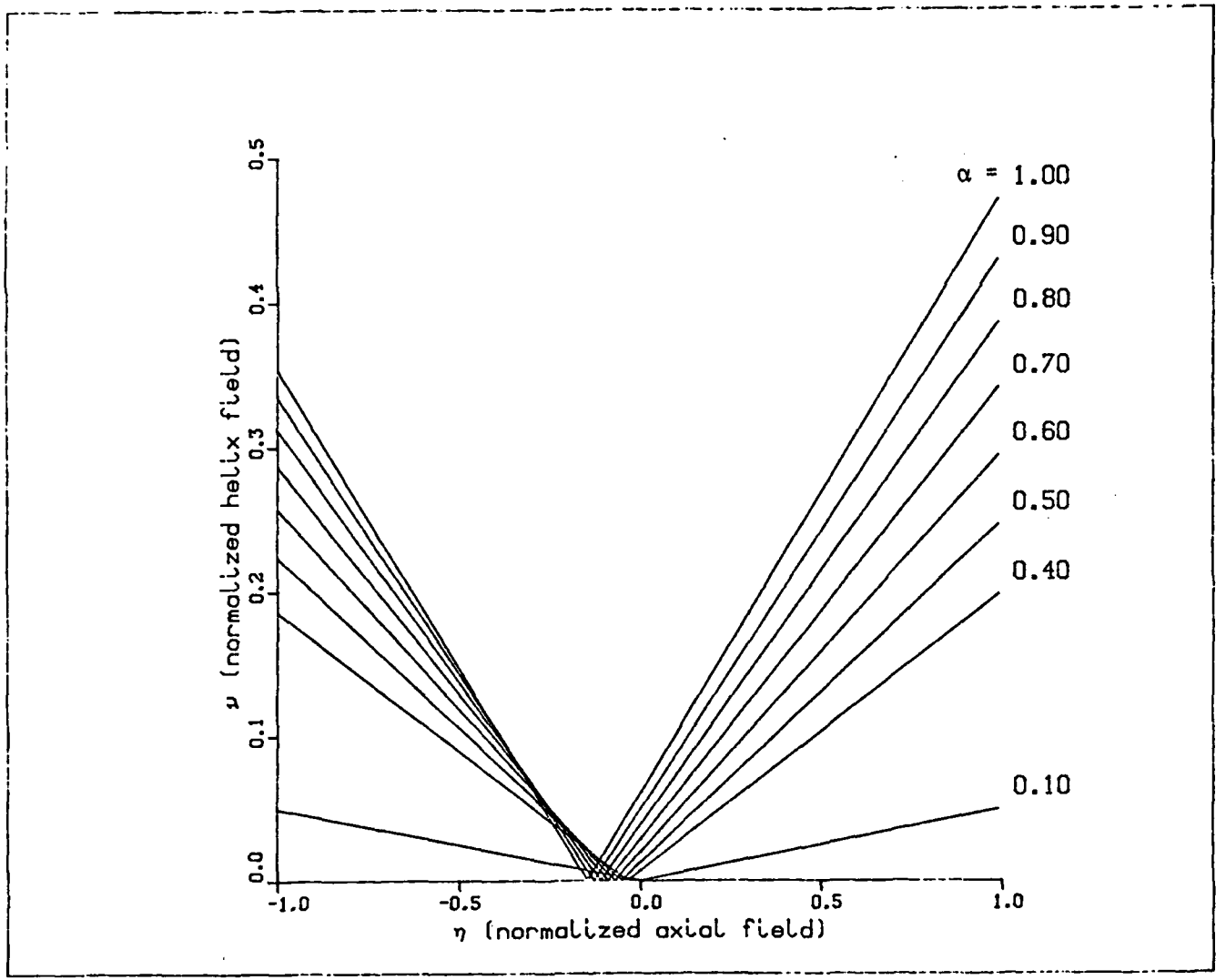

Figure 2-6 Scaling of normalized fields and velocity ratio for a helix with a nonadiabatic entrance. A beam with no initial transverse velocity is assumed and the α's are the peak values.

where

$$A = A_{max},\ p^2 = (\xi - A)^2 + \Gamma^2,\ q^2 = \xi^2 + \Gamma^2$$

$$\mu = \frac{1}{2}\left(\frac{A^2 - (p-q)^2}{pq}\right)^{1/2},\ \xi = \mathrm{Re}(A^{\pm}),\ \Gamma = \mathrm{Im}(A^{\pm})$$

K is the complete elliptic integral of the first kind,

and $A^{\pm}$ = complex conjugate roots of the cubic.

Solutions can also be obtained for $\eta + A/2 < 0$, but the calculations are more complex[6,10].

Analysis of the ideal helix field H-gun has led us to a set of design curves for achieving specific α's and the realization that the gyroresonance can be used to greatly reduce the required helix field. Thus, the generation of high α beams is possible by exploiting the gyroresonance effect. The question of whether beams generated in this manner will be of sufficient quality will be addressed in Section 4 after improvements are made in the helical field model.

SECTION 3
REALISTIC HELIX FIELDS

The previous section has shown that large transverse velocities can be generated with reasonable helix field magnitudes. The H-gun thus satisfies one of the criteria for use in gyro-devices. The issue which remains to be explored is beam quality. In order to examine beam quality in H-guns, more accurate models of the helix field must be used. Velocity spreads occur when particles experience different forces, depending on their position in the beam. The ideal helix model applies the same force to all particles in a cross section and, thus, is inadequate for studying the helix induced velocity spreads.

The exact field produced by an infinite bifilar helical winding of infinitely thin wires has been known for some time[15,4]. Equations for the fields along with the two simplest approximations are shown below.

BIFILAR HELIX MAGNETIC FIELDS

$$B_r = B_0 \sum n K_n'(n k_w a) I_n'(n k_w r) \sin n(\theta - k_w z)$$

$$B_\theta = B_0 \sum \frac{n}{k_w r} K_n'(n k_w a) I_n(n k_w r) \cos n(\theta - k_w z)$$

$$B_z = -B_0 \sum n K_n'(n k_w a) I_n(n k_w r) \cos n(\theta - k_w z)$$

Where $\sum = \sum_{n=1,3,5,\cdots}^{\infty}$, $B_0 = \frac{8 a k_w^2}{c} I$, $k_w = \frac{2\pi}{L}$, a = helix radius

The First Order Fields

$$B_r = B_0 K_1'(k_w a) I_1'(k_w r) \sin(\theta - k_w z)$$

$$B_\theta = B_0 K_1'(k_w a) \frac{I_1(k_w r)}{k_w r} \cos(\theta - k_w z)$$

$$B_z = -B_0 K_1'(k_w a) I_1(k_w r) \cos(\theta - k_w z)$$

On Axis (Set $\theta = \frac{\pi}{2}$)

$$B_x = B_\perp \cos k_w z$$

$$B_y = B_\perp \sin k_w z$$

$$B_z = 0$$

$$B_\perp = \frac{1}{2} B_0 K_1'(k_w a)$$

The I and K functions are the modified Bessel functions of the first and second kind respectively. (Sets of coils will not be considered here in detail to avoid unnecessary complications. This refinement is taken into account in the numerical calculations.) Along with the presence of odd harmonics, there are two important departures from the ideal field. The first of these is the radial variation in the field which occurs through the I and I' functions. The second is that the direction of the field depends on the radius and phase since the radial dependence of the B_r and B_θ components is not the same. A plot of the dependence of the first order field magnitude on radius and phase is shown in Figure 3-1 for a 3 cm period helix. Note that the variation increases with radius.

In addition to the more accurate expressions for the field in a uniform radius helix, there are several factors which must be considered when modeling actual helices. Since a laboratory helix can not be infinite, end effects will have to be taken into account. Also, if the radius of the windings is flared to taper the entrance field, then the uniform radius equations are *no longer* completely valid and corrections must be made. If the field taper is very gradual (over at least five helix periods), an adiabatic approximation can be made (see Figure 2-2). The zero divergence requirement on the helix field, $\nabla \cdot \underline{B}_h = 0$, can be satisfied by adding terms to B_r and B_θ which depend on the derivative of the field magnitude with respect to axial distance. If the field taper is not gradual, then substantial differences occur and numerical methods must be used to evaluate the field. This case will not be considered here.

End effects in a uniform radius helix can be investigated by direct integration[16,17] of the Biot-Savart equation. There are two problems which must be examined. One is the effect caused by ending the helical windings. By this we mean that the helix no longer extends from $-\infty$ to ∞ but starts at some Z_0. The lack of coils for $Z < Z_0$ leaves terms in the equations for the field due to contributions from the $Z > Z_0$ coils which would otherwise be cancelled.

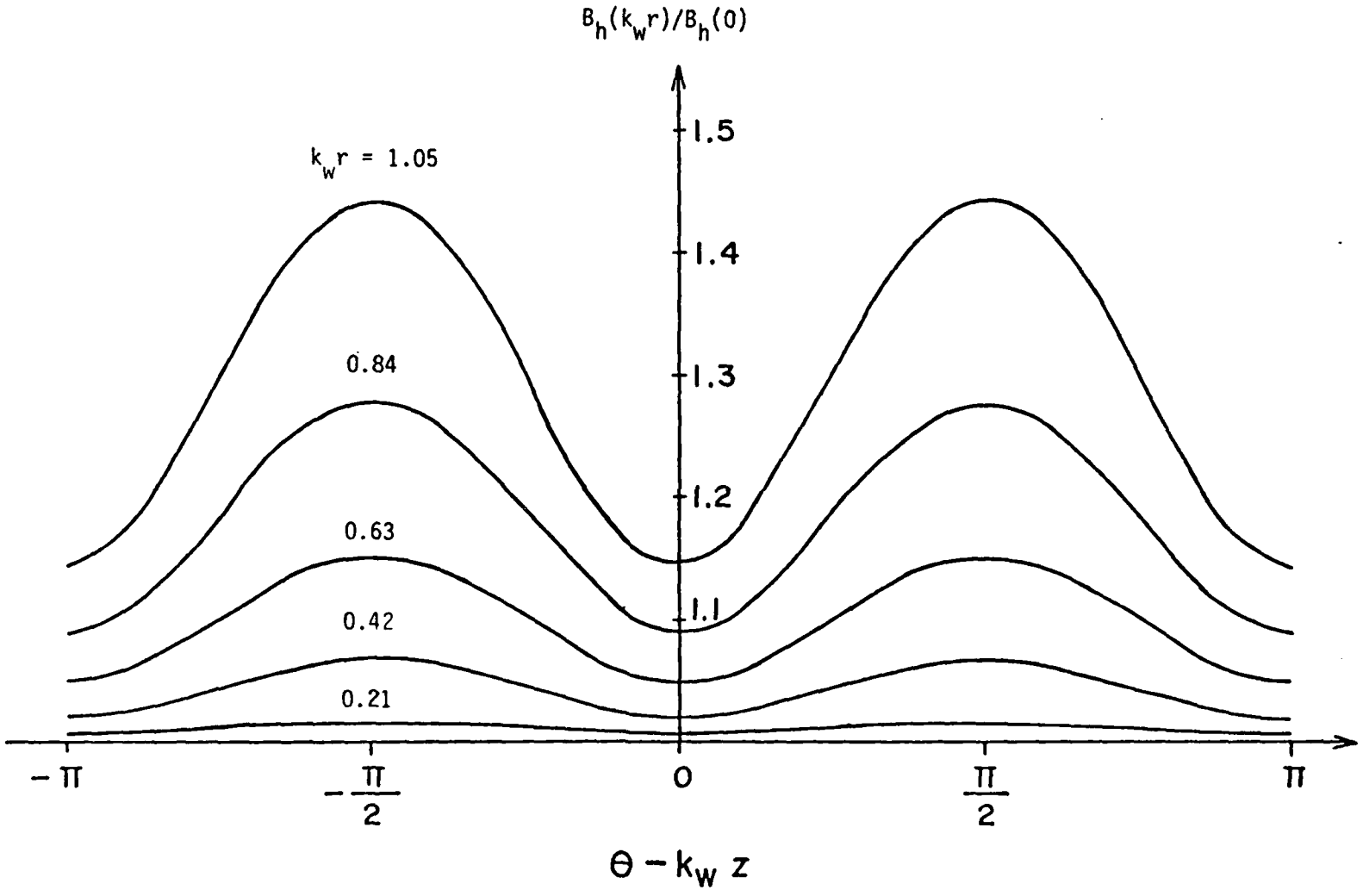

Figure 3-1 Variation in the magnitude of the first order transverse field of a bifilar helix relative to the field magnitude on axis.

The other effect is caused by the way in which the helical windings are joined at the end to complete the current circuit. The equations for the on-axis fields of a uniform radius helix which starts at z = 0 and extends to ∞ are shown below.

$$B_x = b_o\{(HC(\varepsilon,\xi) - K_1'(\varepsilon))\sin\xi + \frac{\pi}{2}(I_1'(\varepsilon) - L_1'(\varepsilon) + \frac{2}{\pi\varepsilon} - \frac{2}{\pi}HS(\varepsilon,\xi))\cos\xi - (\varepsilon^2 + \xi^2)^{-1/2}\}$$

$$B_y = b_o\{-(HC(\varepsilon,\xi) - K_1'(\varepsilon))\cos\xi + \frac{\pi}{2}(I'(\varepsilon) - L_1'(\varepsilon) + \frac{2}{\pi\varepsilon} - \frac{2}{\pi}HS(\varepsilon,\xi))\sin\xi\}$$

where $b_o = \varepsilon k_w I(\text{amps})/5$, $\varepsilon = k_w a$, $\xi = k_w z$, a = helix radius

I, K are the modified Bessel functions, L is the modified Struve function

$$HC(\varepsilon,\xi) = \int_o^\xi \frac{(1 + \varepsilon^2 + x^2)\cos x\,dx}{(\varepsilon^2 + x^2)^{3/2}}\text{, helix cosine integral,}$$

and

$$HS(\varepsilon,\xi) = \int_o^\xi \frac{(1 + \varepsilon^2 + x^2)\sin x\,dx}{(\varepsilon^2 + x^2)^{3/2}}\text{, helix sine integral.}$$

The following properties of HC and HS are useful in examining these equations:

$$HC(\varepsilon,|\xi|) = -HC(\varepsilon,-|\xi|)$$

$$HS(\varepsilon,|\xi|) = HS(\varepsilon,-|\xi|)$$

$$HC(\varepsilon,0) = HS(\varepsilon,0) = 0$$

$$\lim_{\xi\to\infty} HC = -K_1'(\varepsilon), \lim_{\xi\to\infty} HS = \frac{1}{\varepsilon} + \frac{\pi}{2}\left(I_1'(\varepsilon)-L_1'(\varepsilon)\right) .$$

Note that B_x is no longer zero at $z = 0$ and that a nonsinusoidal term occurs. B_y has picked up a $\sin(k_w z)$ dependence, and since HC = 0 at $\xi = 0$, the value of B_y is half the infinite helix value. As $\xi \to \infty$, the term involving HC goes to $-2K_1'(\varepsilon)$ which is the infinite helix value. The term involving HS goes to zero, and the on-axis infinite helix field is recovered. As $\xi \to -\infty$, HS does not change sign, so that term still goes to zero. However, HC does flip sign so that term also goes to zero, and the helix field dies out.

In order to close the current path for the semi-infinite helix, we will assume that at the end of the helix one of the windings is split into two wires and connected to the other winding by wrapping the wires in opposite directions. This produces the following field on axis:

$$\underline{B}_{loop} = b_o \frac{\xi}{(\varepsilon^2 + \xi^2)^{3/2}} \hat{e}_y .$$

When this term is added to the helix field, both the B_x and B_y terms have nonsinusoidal components. The B_x component, however, dominates since it has a $(\varepsilon^2 + \xi^2)^{-1/2}$ dependence. The B_x and B_y components for the combined fields are plotted in Figures 3-2 thru 3-4 for three ratios of helix radius to period. Clearly, the perturbation in B_x

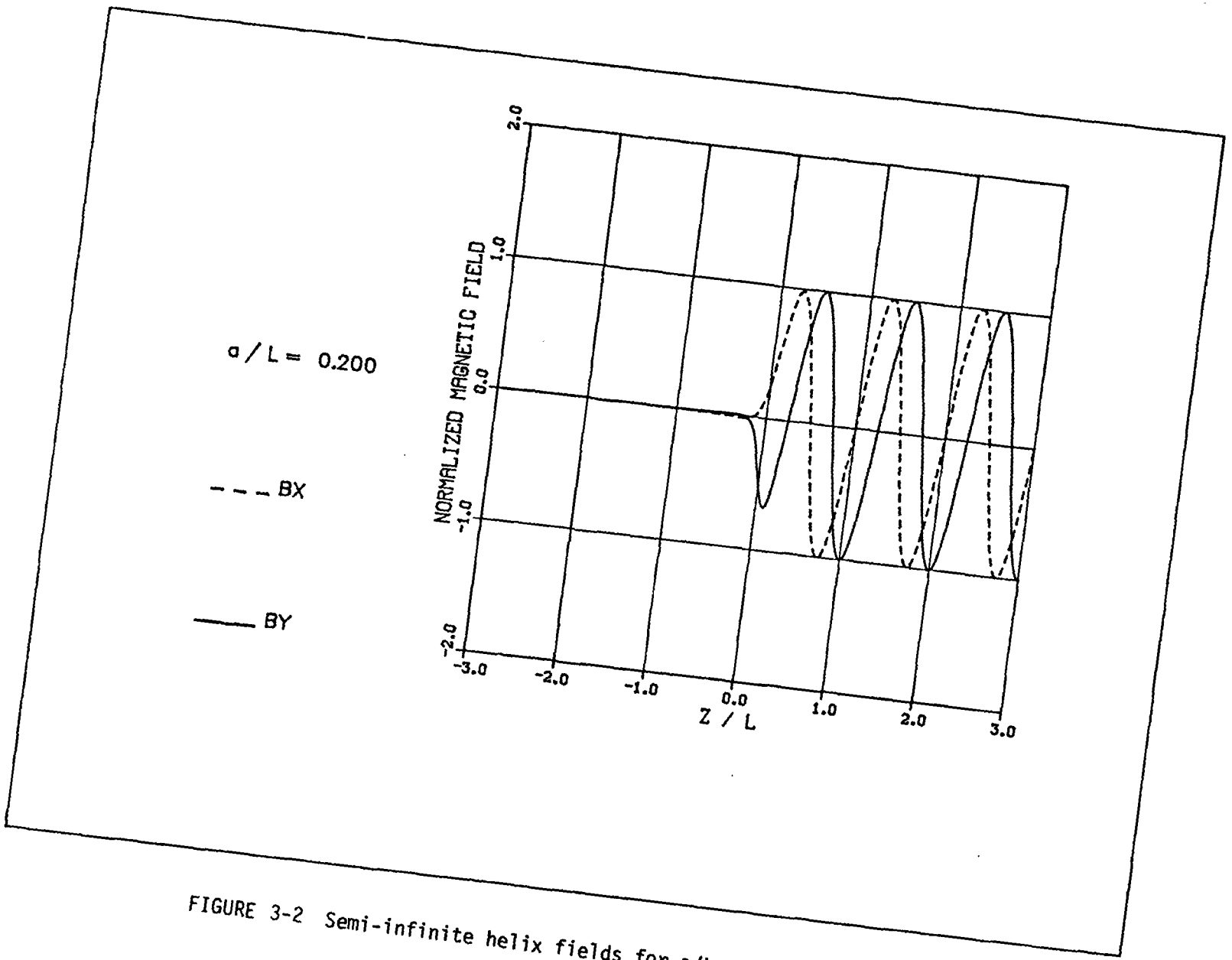

FIGURE 3-2 Semi-infinite helix fields for a/L=.2

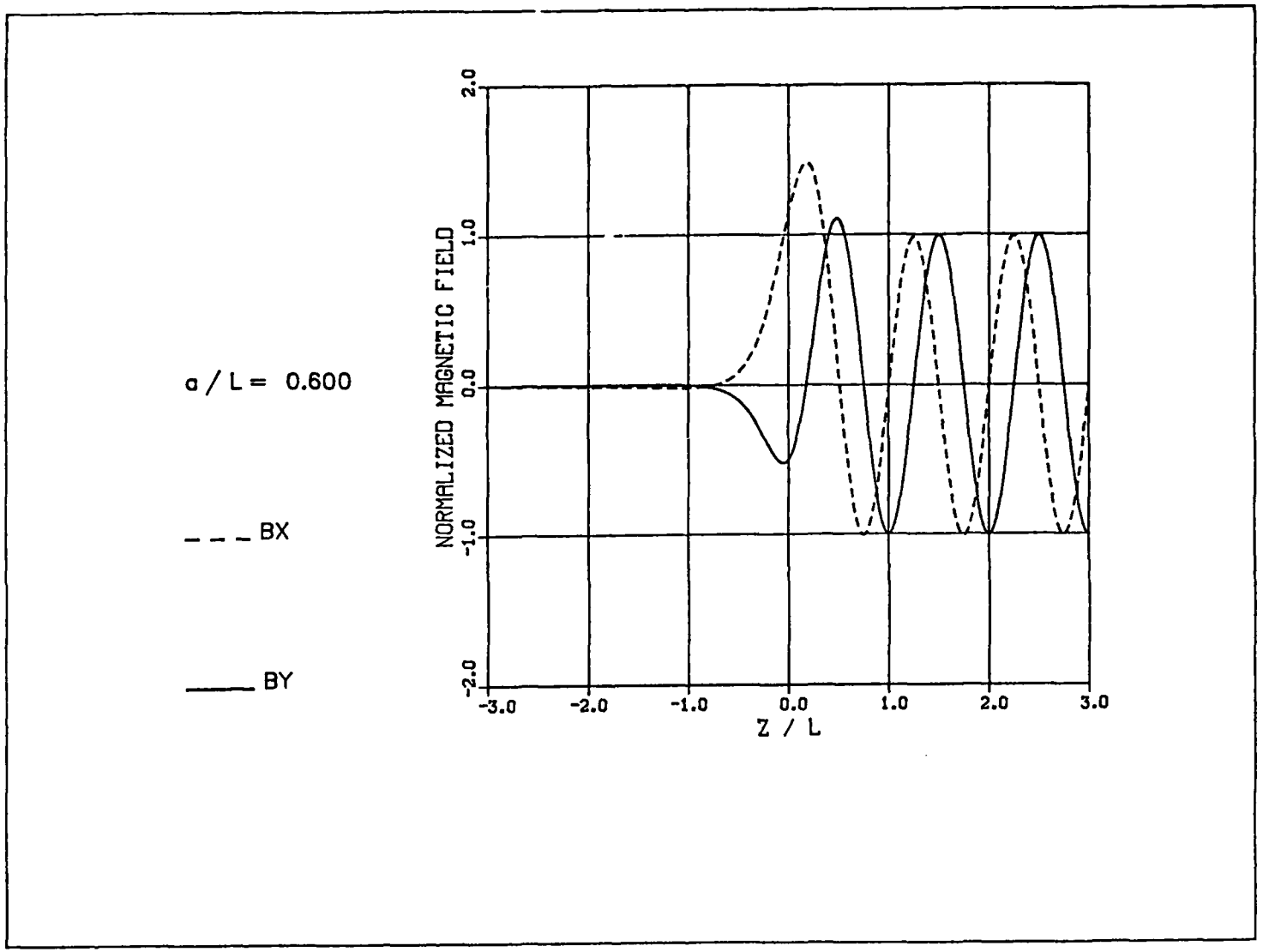

FIGURE 3-3 Semi-infinite helix fields for a/L=.6

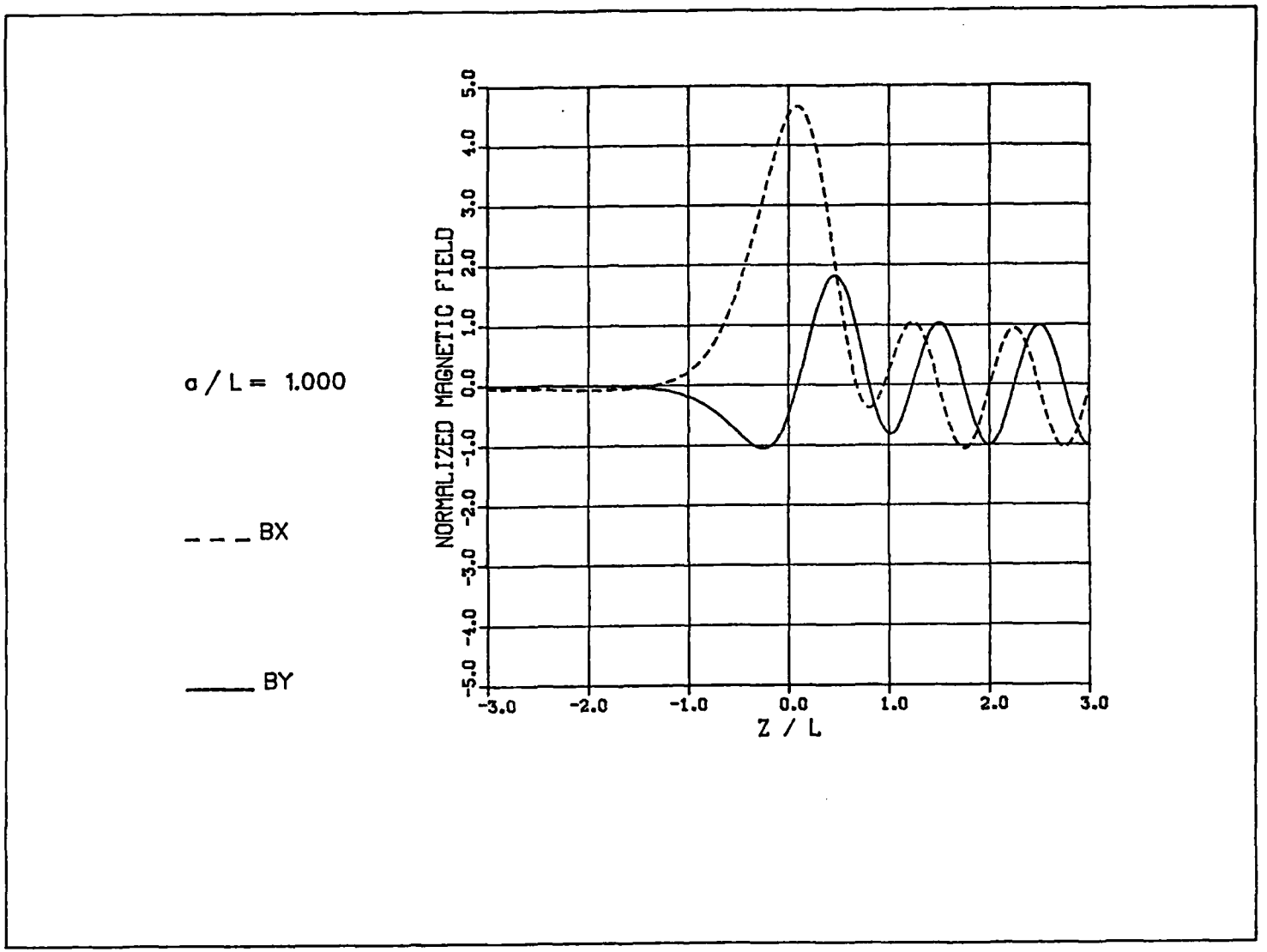

FIGURE 3-4 Semi-infinite helix fields for a/L=1.0

dominates and becomes much larger than the infinite field value for large ε's. The normalized field magnitudes are compared in Figure 3-5. For large ε's the entrance perturbation is not only large, but extends over 2-3 periods. For $\varepsilon \lesssim 2$, however, very sharp, nonadiabatic transitions can be achieved.

Investigation of beam quality in a semi-infinite helix would require solving the fields everywhere in space. One or two radii into the helix the field will closely approximate the infinite helix field off-axis, but the region around the helix entrance may be considerably different. Solution of this problem is certainly possible using an orthogonal function expansion in cylindrical coordinates. Unfortunately time did not permit the completion of this work or inclusion of the on-axis fields in the numerical calculations.

The gradients of the helix field generate spreads in velocity over the beam cross section. In addition to the variation of the off-axis field in the uniform section, one must consider the gradients produced by the helix end effects. The uniform section gradients are driven by the $I_1(k_w r)$ terms. These can be kept small by choosing a helix period such that $k_w r_{beam} \ll 1$. The end effects present a different problem. As we have seen, the relative effect of ending the helix can be reduced by keeping a/L small (see Figures 3-2 thru 3-4); however, the gradients associated with this may be high over a small region. Requiring $r_{beam}/a \ll 1$ is too restrictive a condition on the beam. For the nonadiabatic helix, this is a problem that will simply have to be tolerated. For the tapered radius adiabatic helix, the end gradients are greatly reduced and present only a minor problem, provided a/L is kept reasonably small in the uniform section.

Additional features of realistic helix fields which must be considered are the harmonic content of the field and the current required to generate the desired field magnitude. As shown previously, the field

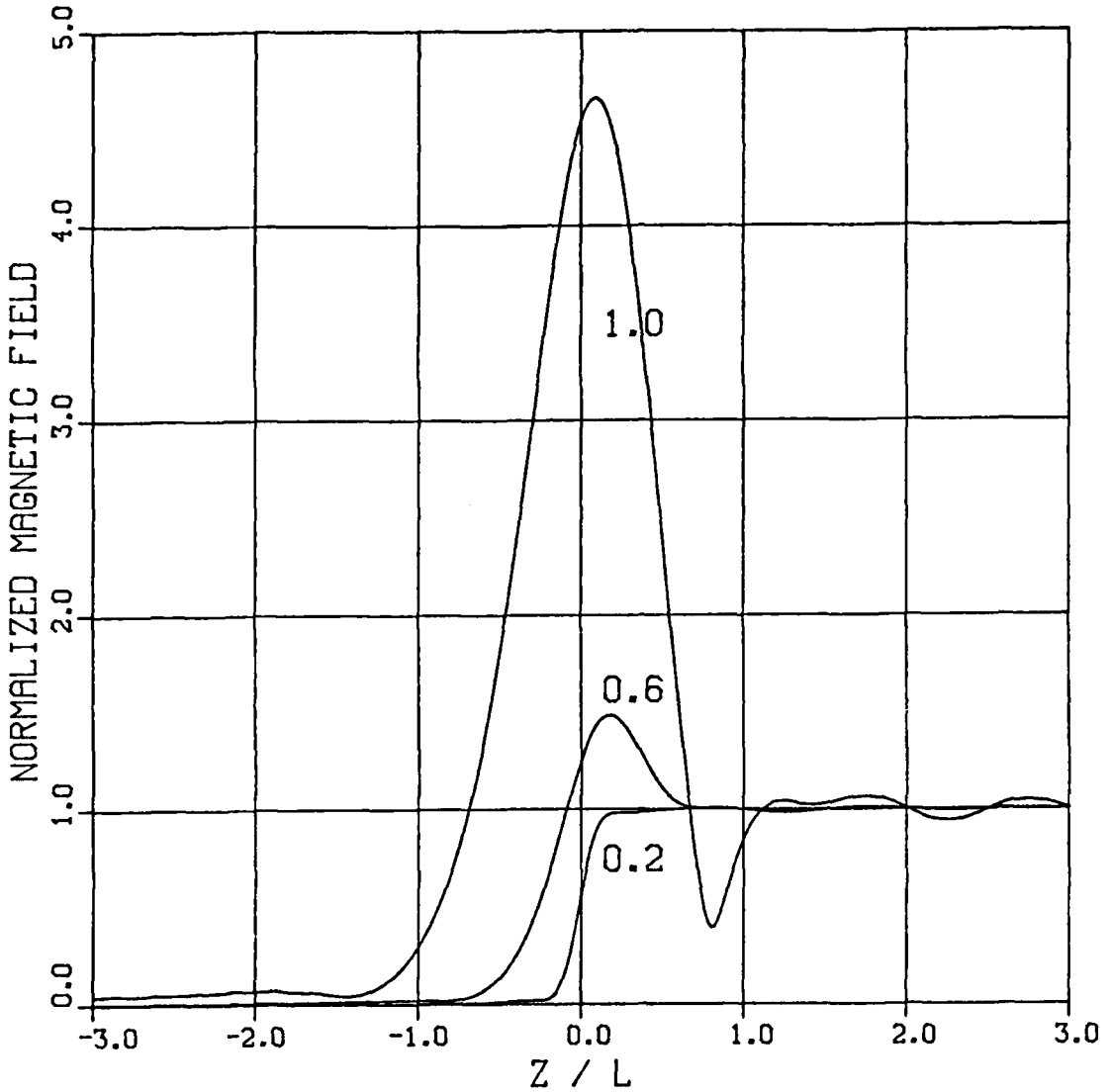

FIGURE 3-5 Comparison of End Effects in a semi-infinite helix for three radius-to-period ratios.

from a thin wire bifilar helix has many odd harmonics. Actual H-guns will use coils of wire in the helix, and hence the harmonic content will depend on the coil geometry. For an infinite helix, if the coils are assumed to be centered symmetrically on z=0, then the following equation can be derived for the harmonic amplitudes:

$$A_n = \sum \cos\,(nk_w z) \sum nk_w a(z)\, K_n'\,(nk_w a(z)) \ ,$$

where the sums are over the wire positions in the coil cross section, each wire is assumed to carry the same current, and z is measured relative to the center of the coil (refer to Figure 3-6 below). Using this formula it is easy to show that a rectangular coil cross section extending from z = -L/6 to z = L/6 will greatly reduce or eliminate the third harmonic. Since $K_n'\,(nk_w a)$ drops rapidly with increasing harmonic number, elimination of the third harmonic essentially eliminates all of the higher harmonics. If the beam approaches the helix radius, this is no longer true and the higher harmonics must be accounted for. For a solid beam as long as

$$r_\perp = \alpha_{helix}/k_w < a \ ,$$

then harmonics should not be a problem.

The first order helix field magnitude on-axis is given by

$$B_h(o) = 2\, k_w I(amps)\, (k_w a K_1'(k_w a)/5.$$

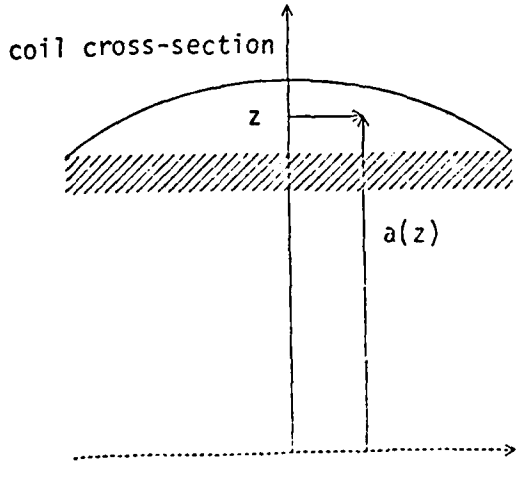

Figure 3-6

As $k_w a$ increases K'_1 exponentially decreases, and if the field is kept at the same value, then the required current rises exponentially. This is a compelling argument for keeping the helix radius small compared to the period. This suggests that H-gun designs should utilize as long a period as possible. This can not be pushed too far, however, because the off-axis shift of the beam increases with increasing period. Physical limits are imposed on this shift by the drift tube and, in addition, the harmonic amplitudes, which grow larger as the radius is increased. Taking these factors into account a reasonable range of operation for H-guns would be

$$0.7 < k_w a < 3 \quad ,$$

depending on the exact parameters of the problem.

SECTION 4
H-GUNS WITH REALISTIC FIELDS

Beam propagation in realistic helix fields was investigated computationally with the TRACK-3 computer code.[12,13] TRACK-3 includes fully relativistic equations of motion and full, three-dimensional fields. The complete bifilar helix fields are included with appropriate modifications for multi-wire coils and adiabatic corrections to the entrance field. For the H-gun study a cold, solid, monoenergetic electron beam was simulated with 62 rays. A uniform axial field and a first order helix field were applied. Both adiabatic and nonadiabatic entrance fields were studied, but a nonadiabatic exit was assumed in all cases. The general features of the beam properties at the exit of the helix will be discussed first. Then specific examples will be given based on the parameters used in a recent H-gun experiment.[1] Throughout this discussion keep in mind that the comparison between the adiabatic and nonadiabatic helix transitions is based on field approximations that are not exactly equivalent in accuracy. For reasons detailed in the previous section, velocity spreads in the nonadiabatic H-gun are slightly lower than they should be.

Most of the characteristics of the adiabatic H-gun can be qualitatively understood based on the ideal orbits and the realistic helix field. The general properties of the adiabatic H-gun were studied using a seven period transition from zero helix field to full magnitude. Details will change according to field profile, number of periods, beam radius, and other factors, but the general observations made here hold for all adiabatic transitions. Important characteristics of the ideal orbits are the instability which occurs for type-I orbits, and the increase in the velocity perturbation as the gyroresonance is approached. Both effects are evident in Figures 4-1 and 4-2 which show the magnitude of the velocity perturbation as functions of the normalized guide and helix

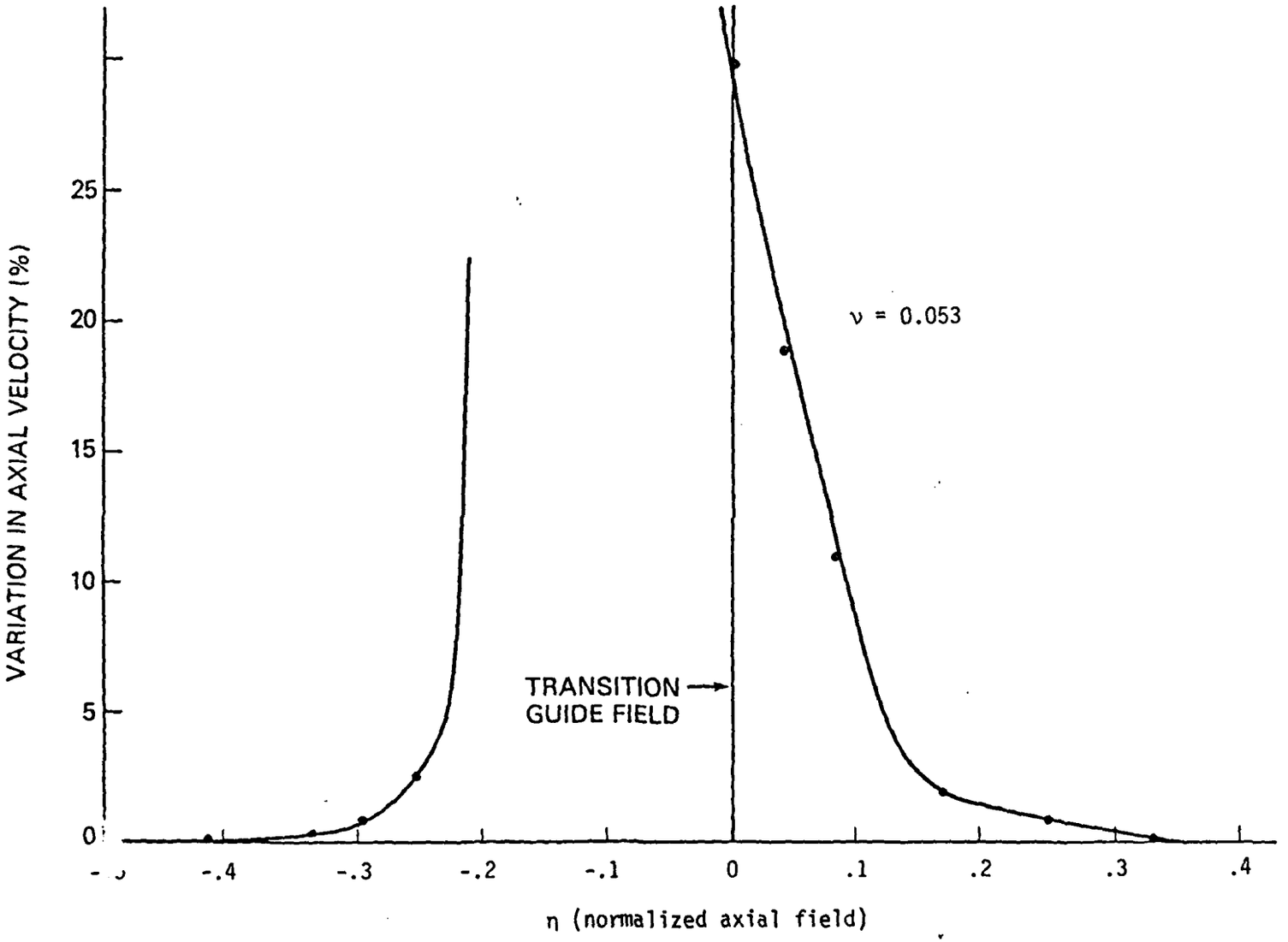

Figure 4-1 Axial velocity perturbation ($2\delta_z/\beta_z$) as a function of proximity to gyroresonance in an adiabatic helix.

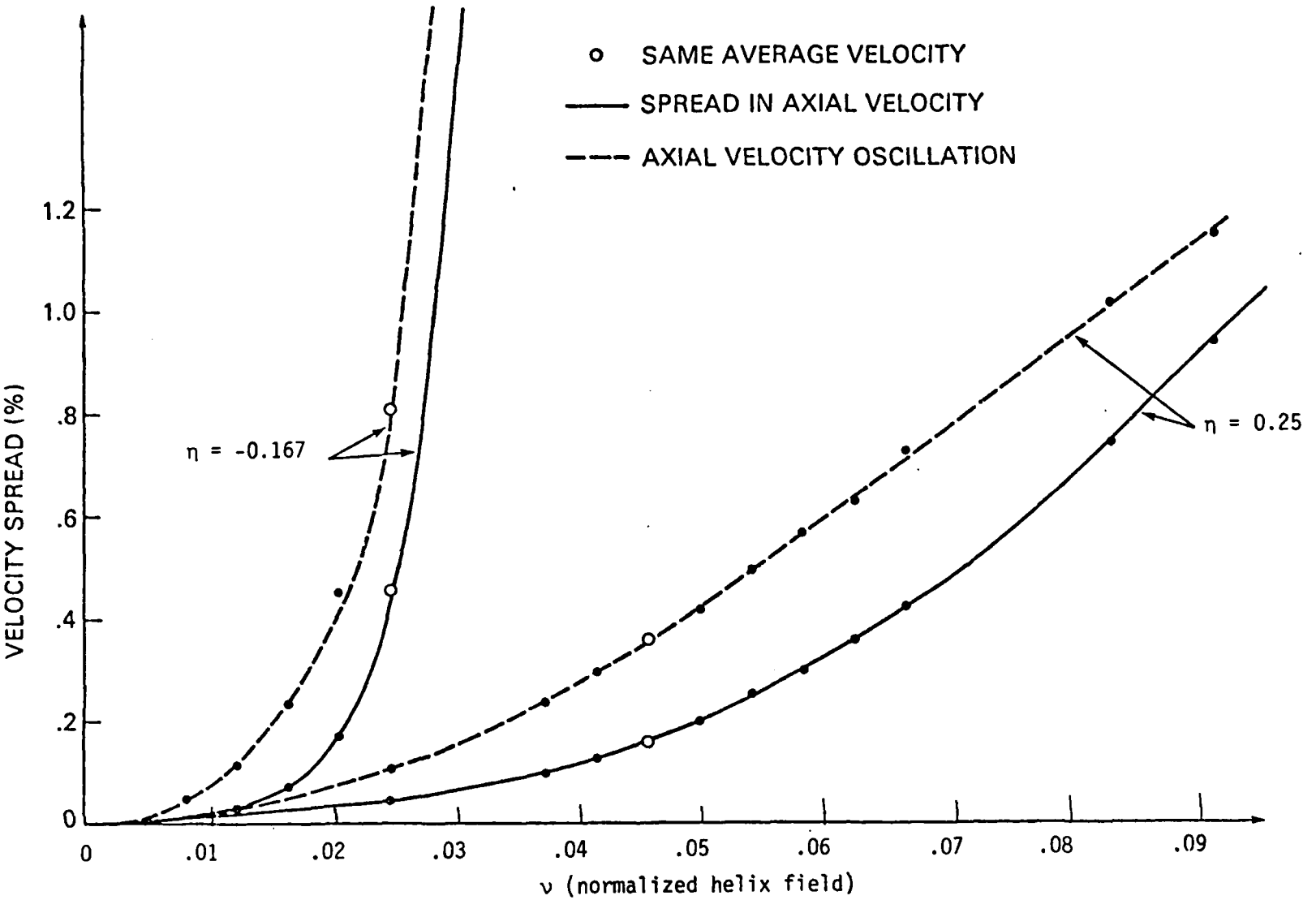

Figure 4-2 Axial velocity $(\sigma(\beta_z)/\beta_z)$ and perturbation (δ_z/β_z) as a function of helix field in an adiabatic helix. Two cases are shown, one below resonance, $\eta = -0.167$, and the other above, $\eta = 0.25$.

fields respectively. The velocity oscillations by themselves are not detrimental to H-gun operation; they simply make the exit α harder to predict. However, remember that the helix field now varies across the beam and the gyroresonance will magnify these field differences. Thus, the same factors which cause the velocity oscillation to increase will give rise to increased velocity spreads. This is shown in Figures 4-2 and 4-3 where the velocity spread is plotted as a function of the helix field and the guide field respectively.

The results of these TRACK-3 calculations can be summarized as follows:

1) Increasing α results in increased velocity spread.

2) Increasing the helix field produces less velocity spread than moving closer to gyroresonance (see circles in Figure 4-2).

3) Operation above gyroresonance is preferable to below for these reasons:

   a) no instability
   b) reduced sensitivity to perturbations
   c) to operate above resonance requires either higher guide fields or longer helix periods; both improve beam quality and stability.

4) Predictions of α based on the ideal approximations and the results from computer calculations are in only modest agreement for the adiabatic case, particularly at high α. This is because of the inability to estimate accurately the perturbation velocity, δ, caused by the adiabatic entrance. This problem is severe around the gyroresonance, resulting in almost nonadiabatic performance. Further from resonance predictions and calculations are in much better agreement.

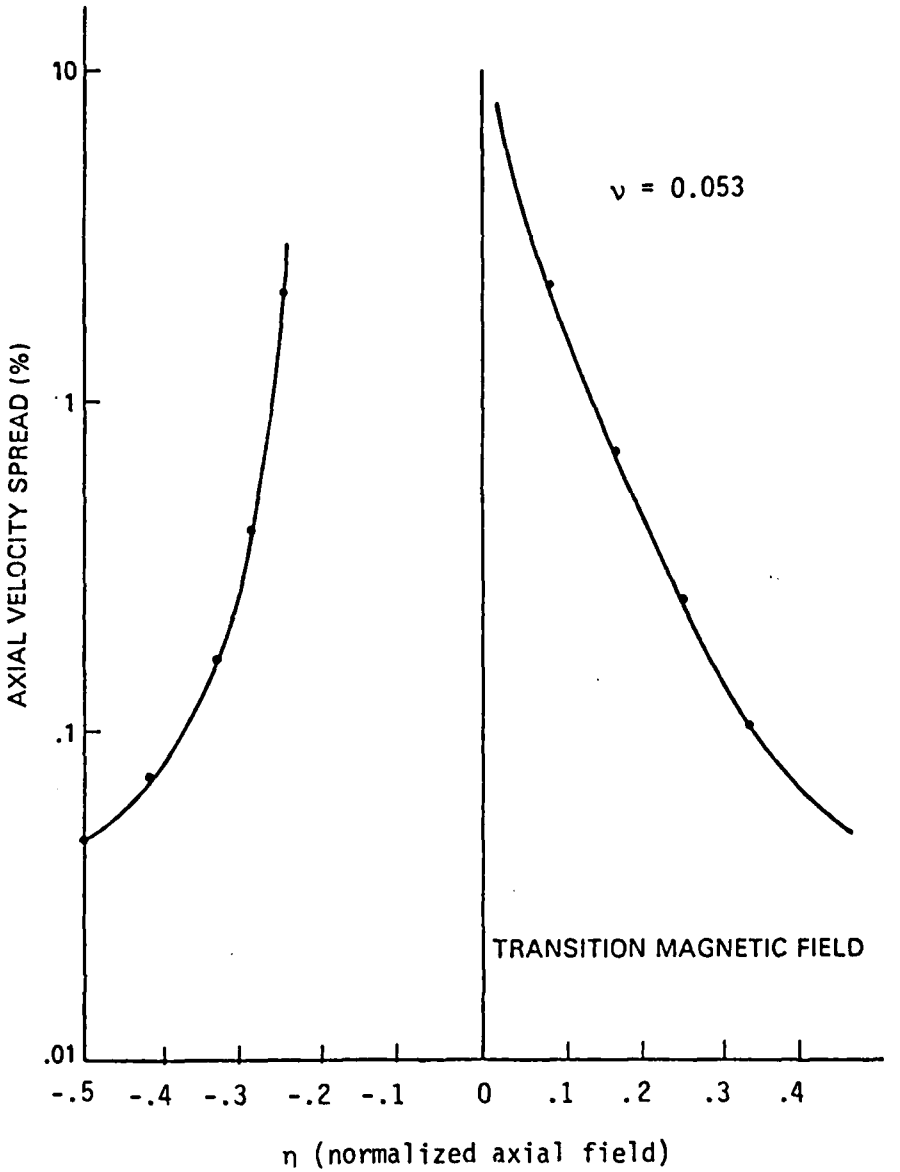

Figure 4-3 Axial velocity spread $(\sigma(\beta_z)/\beta_z)$ as a function of proximity to gyroresonance in an adiabatic helix.

5) The exit α of an adiabatic H-gun is tunable over a wide range provided sufficient helix field magnitude can be generated. Gradual decreases in helix field result in equally gradual decreases in α, and increased helix field results in increased α.

Nonadiabatic H-guns were modelled with an instantaneous increase of the helix field from zero to the full, first-order field of the infinite helix. For $a/L \leq 0.3$, the sharp field rise is probably not a bad approximation. As discussed in Section 3, gradients due to end effects were not included; hence, the velocity spreads should be slightly higher than predicted. Comments (1) - (3) above hold for nonadiabatic H-guns as well as adiabatic ones. The final comments differ for the two cases.

4') Predictions of α for the nonadiabatic H-gun are in good agreement with calculations. Generally the peak calculated α is 5-10% higher due to the increased transverse field off-axis. This better agreement is due to the more accurate treatment of the orbit equation and the beam initial conditions.

5') In the nonadiabatic H-gun, α is generated over a shorter distance and with less helix field than in the adiabatic H-gun. The price one pays for this is a higher velocity spread and less tunability. Remember that in the nonadiabatic case, both α_{max} and the position at which it occurs depend on the fields.

These points will be illustrated by reference to a specific example, that of a recent H-gun experiment at Varian Associates' Palo Alto tube division. The output beam characteristics for the conditions under which the experiment was run[18] are shown in Figures 4-4 and 4-5. The guide field was operated below resonance, and the H-gun was in a nonadiabatic configuration. The beam was extracted well after reaching

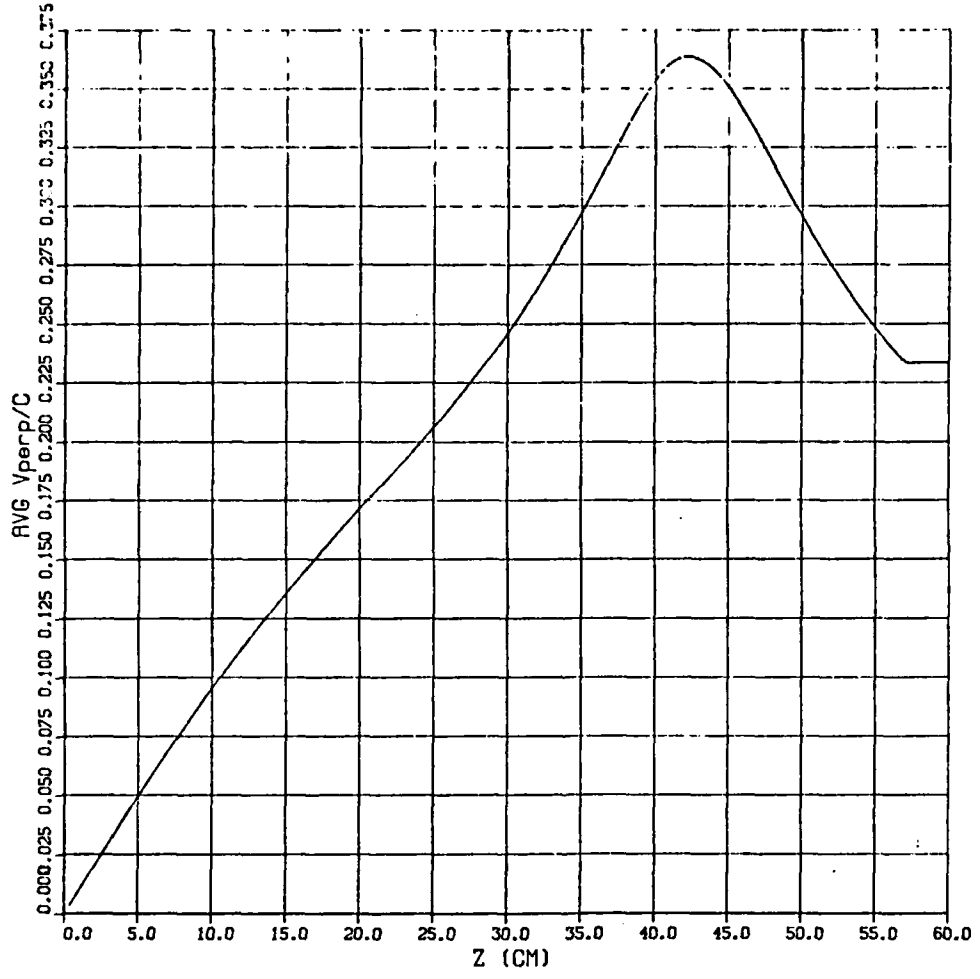

Figure 4-4 Transverse velocity in a nonadiabatic H-gun below resonance. B_z = 723 G, B_h = 20 G. (η = -0.135, ν = .024).

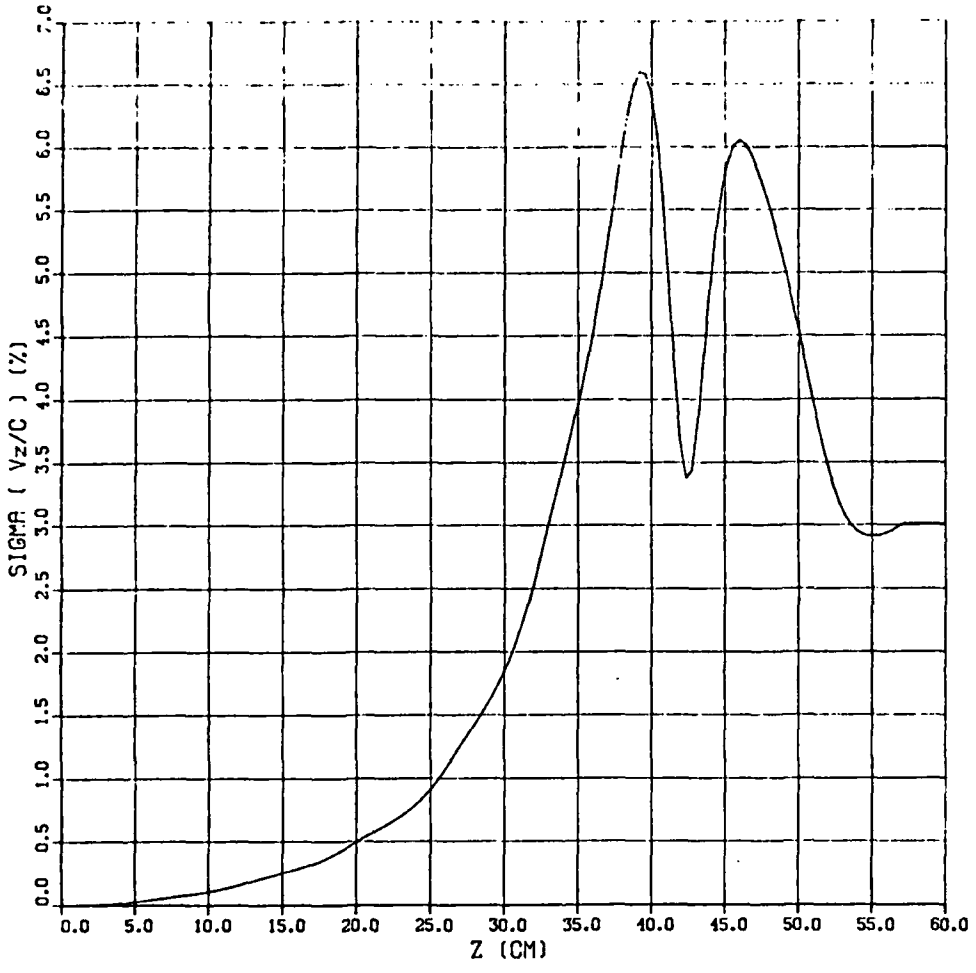

Figure 4-5 Standard deviation of the axial velocity in a nonadiabatic H-gun below resonance. B_z = 723 G, B_h = 20 G. (n = -0.135, ν = .024).

α_{max} with the output shown in the figures being the approximate design α for the experiment. The axial velocity spread at the helix exit is calculated to be approximately 3%; however, in this case since the beam has been allowed to "bounce", the velocity spread is probably higher due to space-charge and other effects. When compressed into the interaction region, the spread would have been much worse. The output for the same helix parameters, but with the guide field raised above gyroresonance, is shown in Figures 4-6 and 4-7. Note that a significant improvement in performance is predicted if the helix is shortened to $\approx$ 25 cm and operated above resonance. For approximately the same α, a velocity spread of 0.8% is predicted. Again this number is low but probably less so than in the first case, since the helix length would be shorter and the orbit would not be allowed to "bounce".

An equivalent adiabatic H-gun designed to operate at the same conditions as used in Figures 4-6 and 4-7 is shown in Figures 4-8 and 4-9. The performance is similar except that the adiabatic helix is longer. The velocity perturbation issue occurs here in the sense that the helix field calculated from the ideal approximation is three times the field needed to give the desired output. The guide field for this case is very close to the gyroresonant value. Note that the output α here is tunable. (Compare the transverse velocity build-up in the two cases.) Lower helix fields will result in correspondingly lower α's and, up to a point, higher fields will result in higher α's. Operation further from the resonance would agree more closely with ideal field calculations.

The next graph, Figure 4-10, illustrates the problems one might encounter in tuning a nonadiabatic H-gun. This run was for the same parameters as for Figures 4-4 and 4-5, except that the helix current was reduced by 38%. One might expect to improve the beam quality by lowering α_{max} to the desired output level and moving α_{max} to the exit. However, by reducing the helix field by 38% the exit α has been reduced by almost 100%, and the peak has been moved from 43 cm to 30 cm. This emphasizes the need for very careful design of nonadiabatic H-guns.

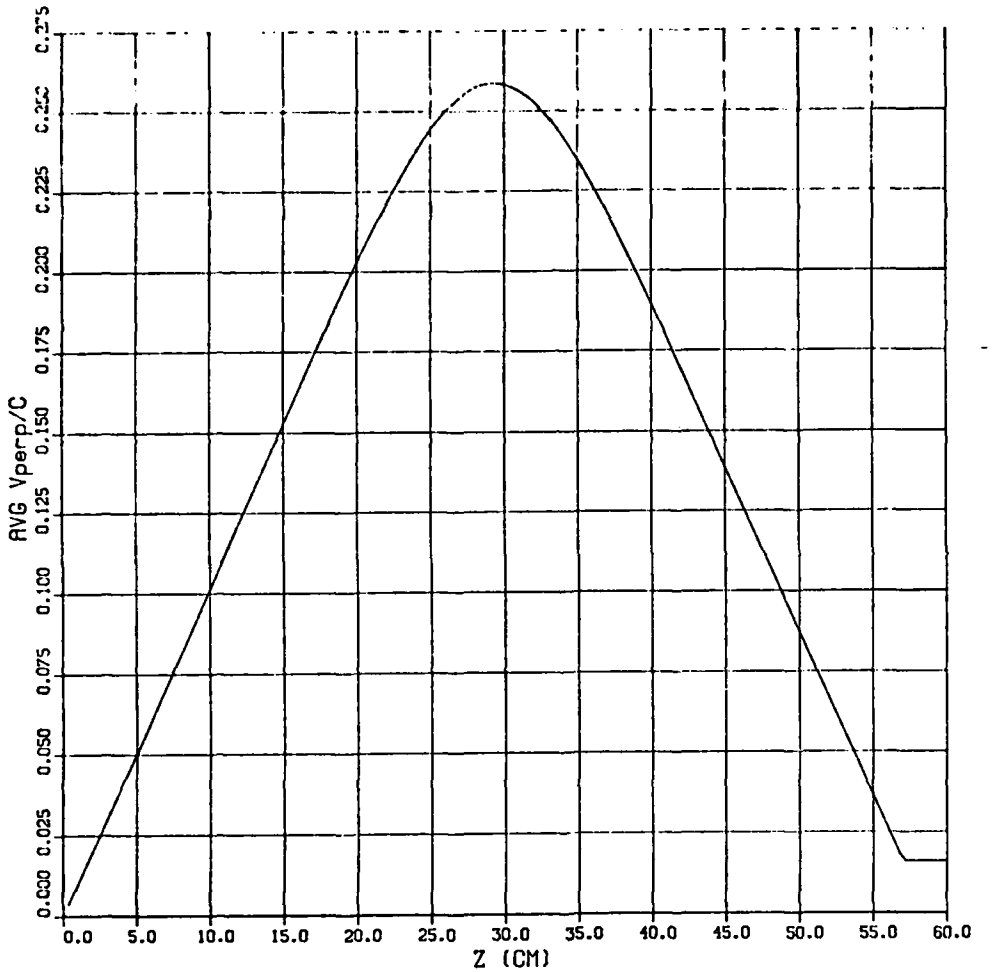

Figure 4-6 Transverse velocity in a nonadiabatic H-gun above resonance. B_z = 836, B_h = 20 G. (η = 0.0, ν = .024).

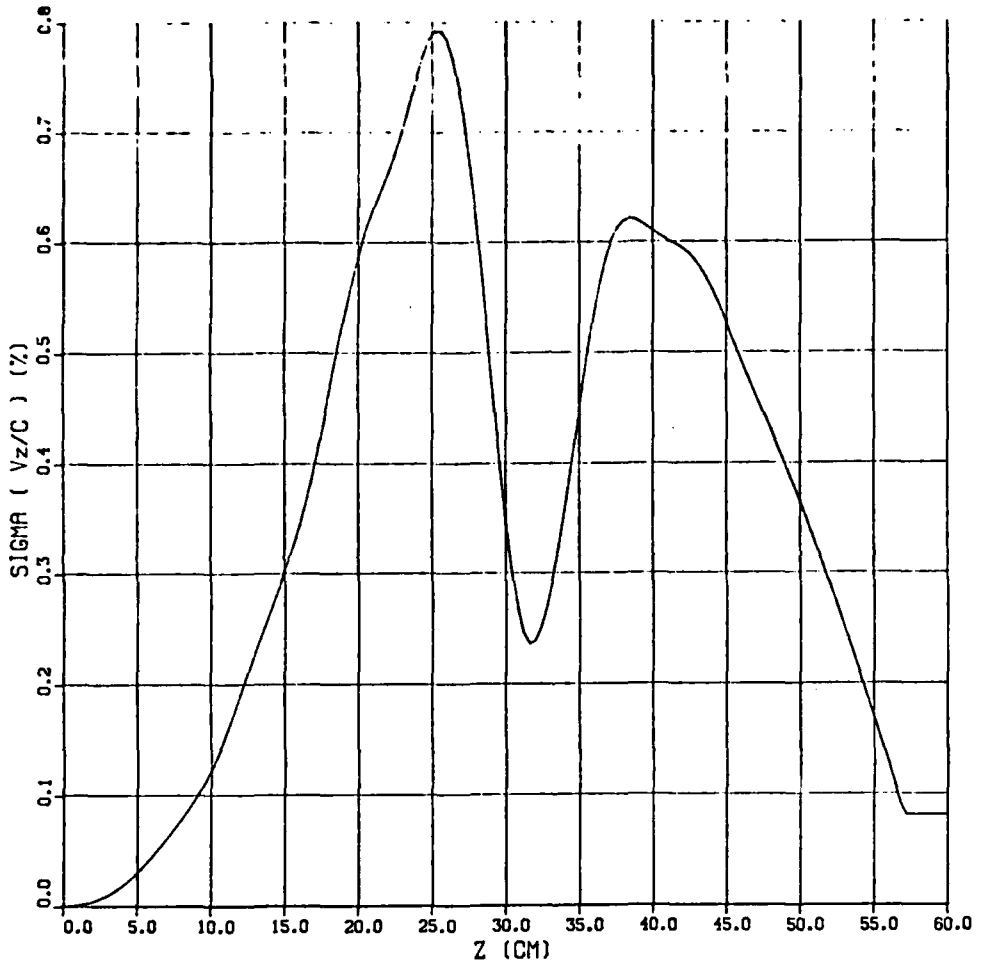

Figure 4-7 Standard deviation of the axial velocity in a nonadiabatic H-gun above resonance. B_z = 836, B_h = 20 G. (η = 0.0, ν = .024).

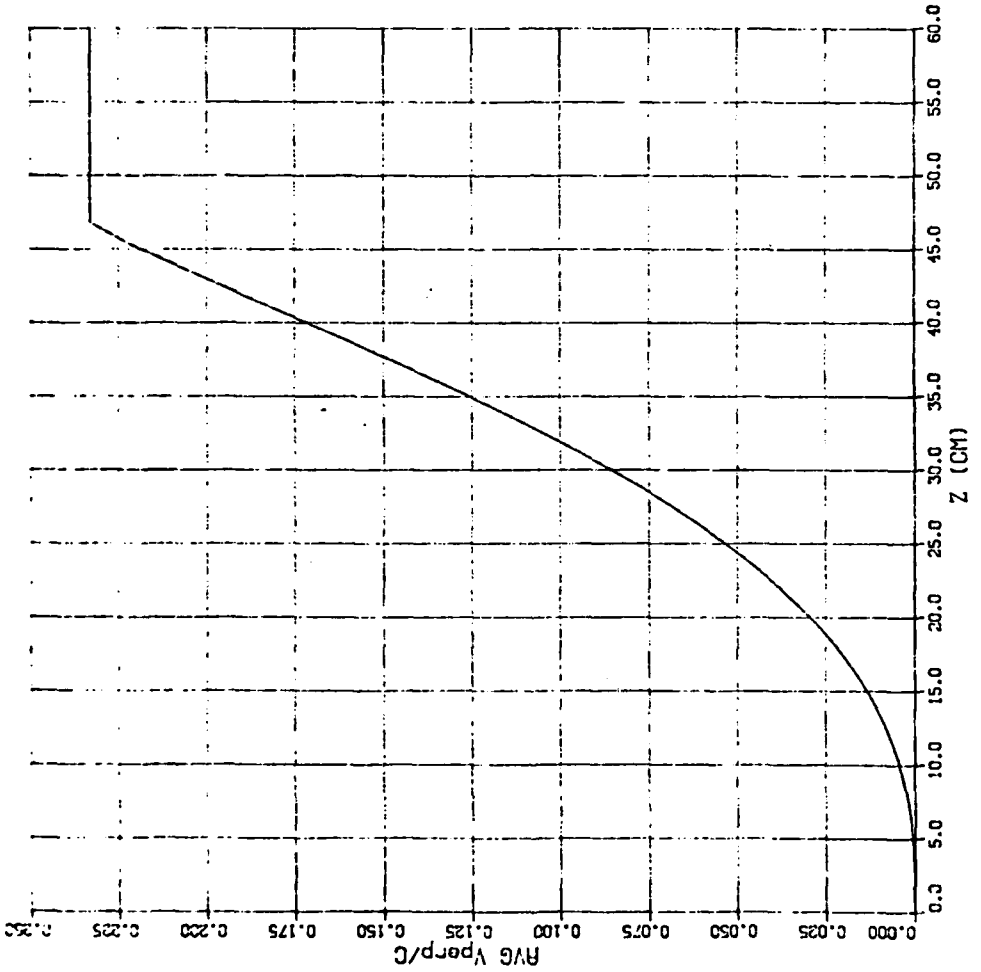

Figure 4-8 Transverse velocity in an adiabatic H-gun above resonance. B_z = 836 G, B_h = 20 G. (η = 0.0, ν = .024).

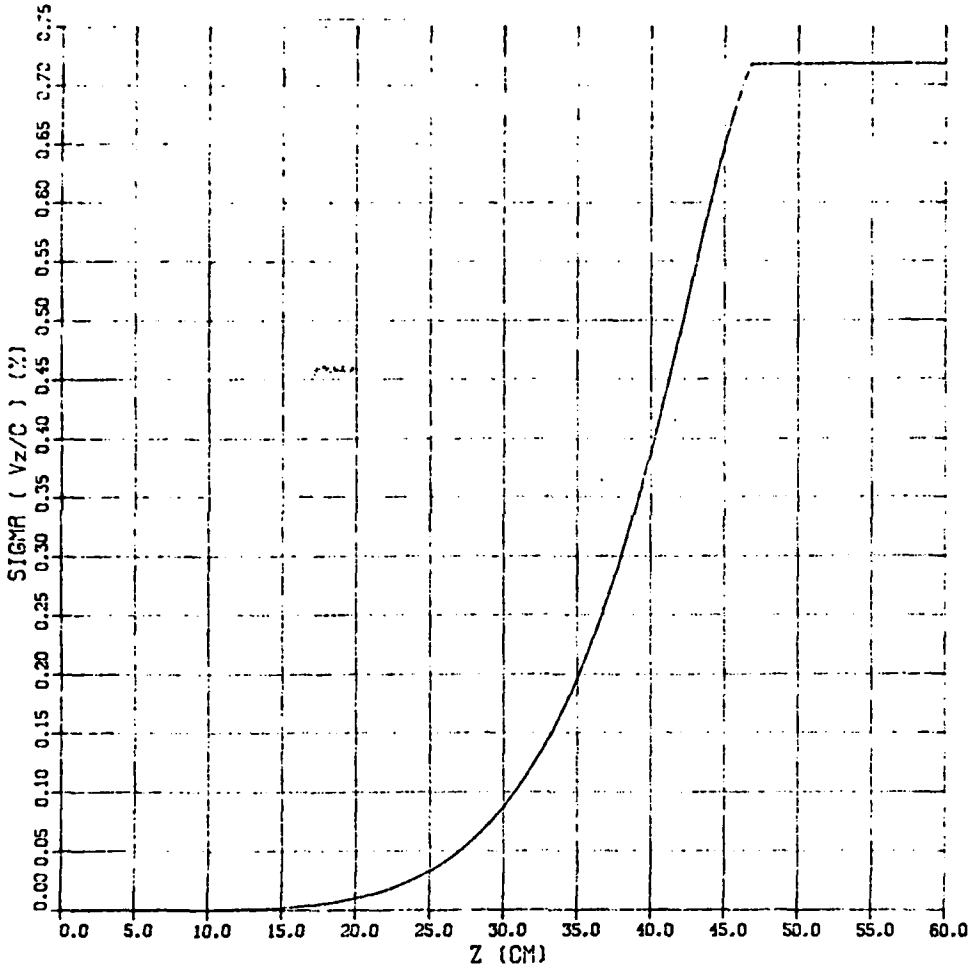

Figure 4-9 Standard deviation of the axial velocity in an adiabatic H-gun above resonance. B_z = 836 G, B_h = 20 G. (η = 0.0, ν = .024).

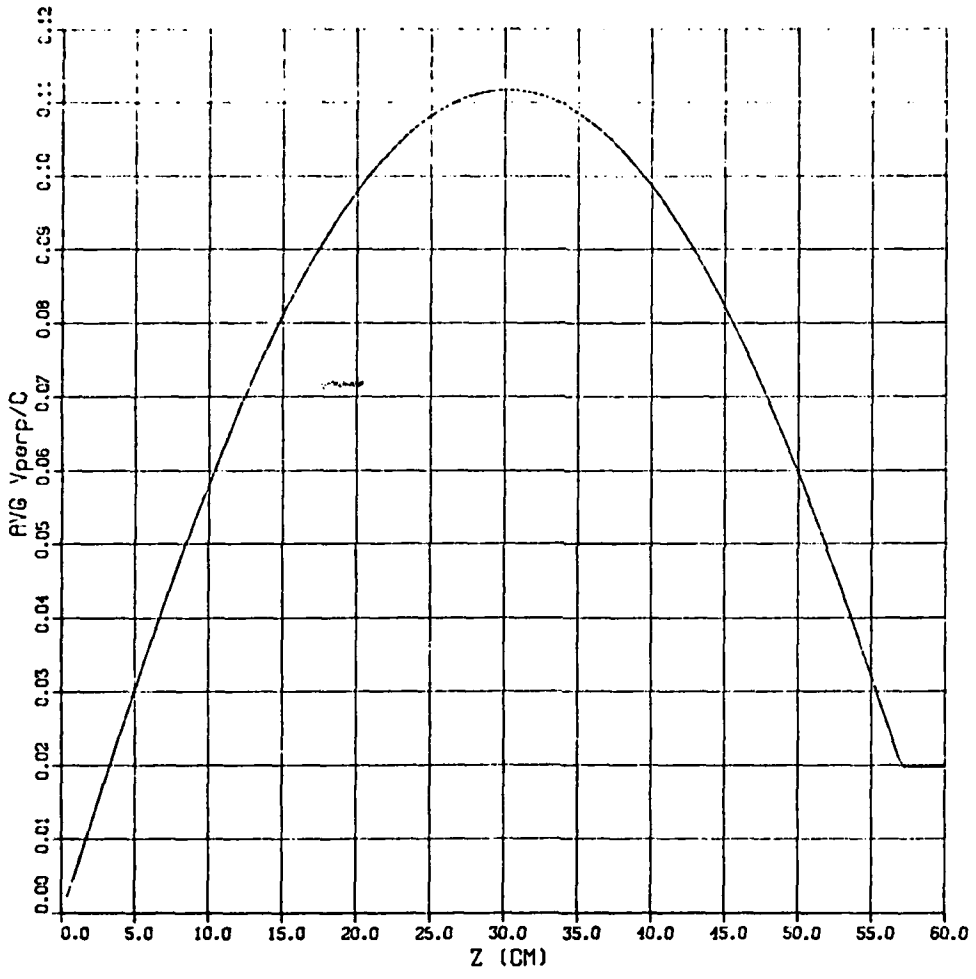

Figure 4-10 Transverse velocity in a nonadiabatic H-gun below resonance. B_z = 723 G, B_h = 12.5 G. (η = -0.135, ν = 0.015).

The last two figures in the sequence (Figures 4-11 and 4-12) show operation of the adiabatic H-gun below resonance (c.f. Figures 4-4, 4-5, 4-6, and 4-7). The quality of the beam is slightly better than the nonadiabatic case, but is inferior to the above resonance adiabatic case. Note that a higher helix field is required, because the axial field is further from resonance.

Some general conclusions about the two types of H-gun designs can be drawn from this data.

1) Experimental investigations of the H-gun should probably use an adiabatic helix designed to allow operation far above resonance as well as close to resonance in order to achieve high beam quality and tunability.

2) If beam quality is the most important consideration, then an adiabatic helix should be used.

3) If compactness and efficient generation of α are the critical factors and only limited tunability is required, then a nonadiabatic design is superior.

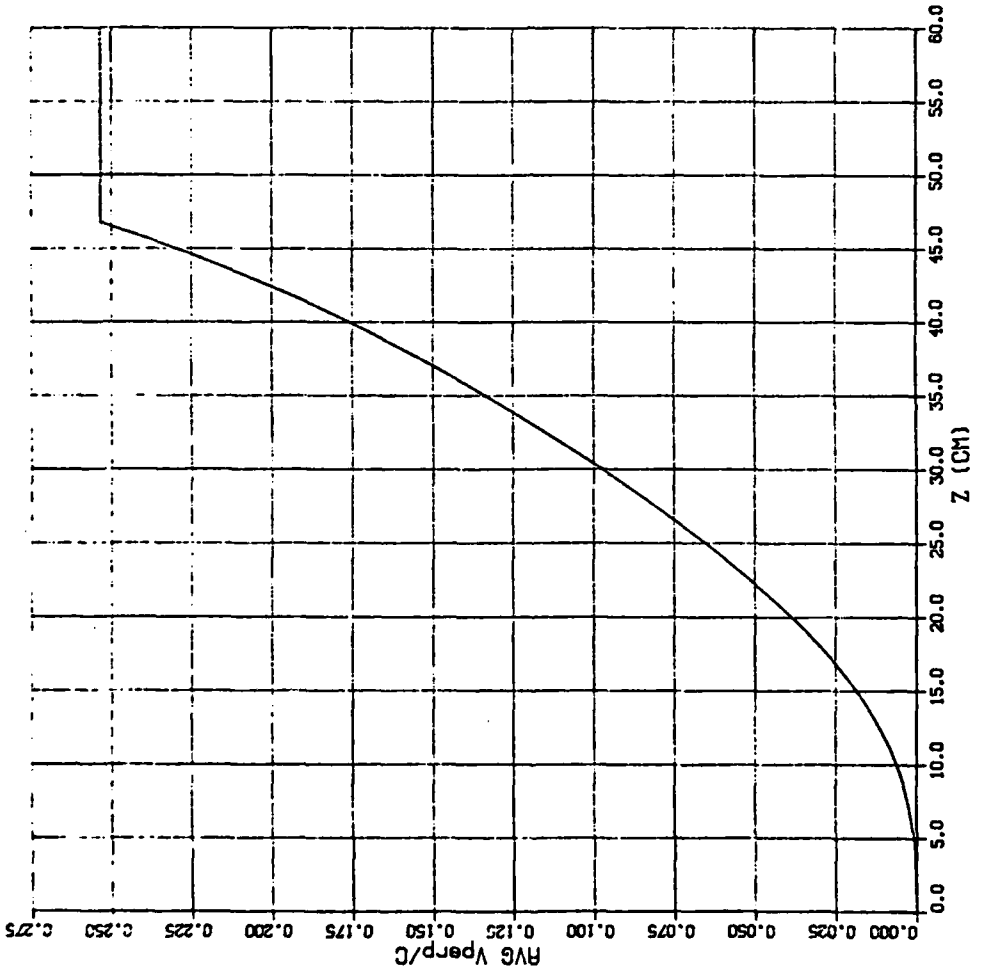

Figure 4-11 Transverse velocity in an adiabatic H-gun below resonance. B_z = 723 G, B_h = 31 G. (n = -0.135, ν = 0.037).

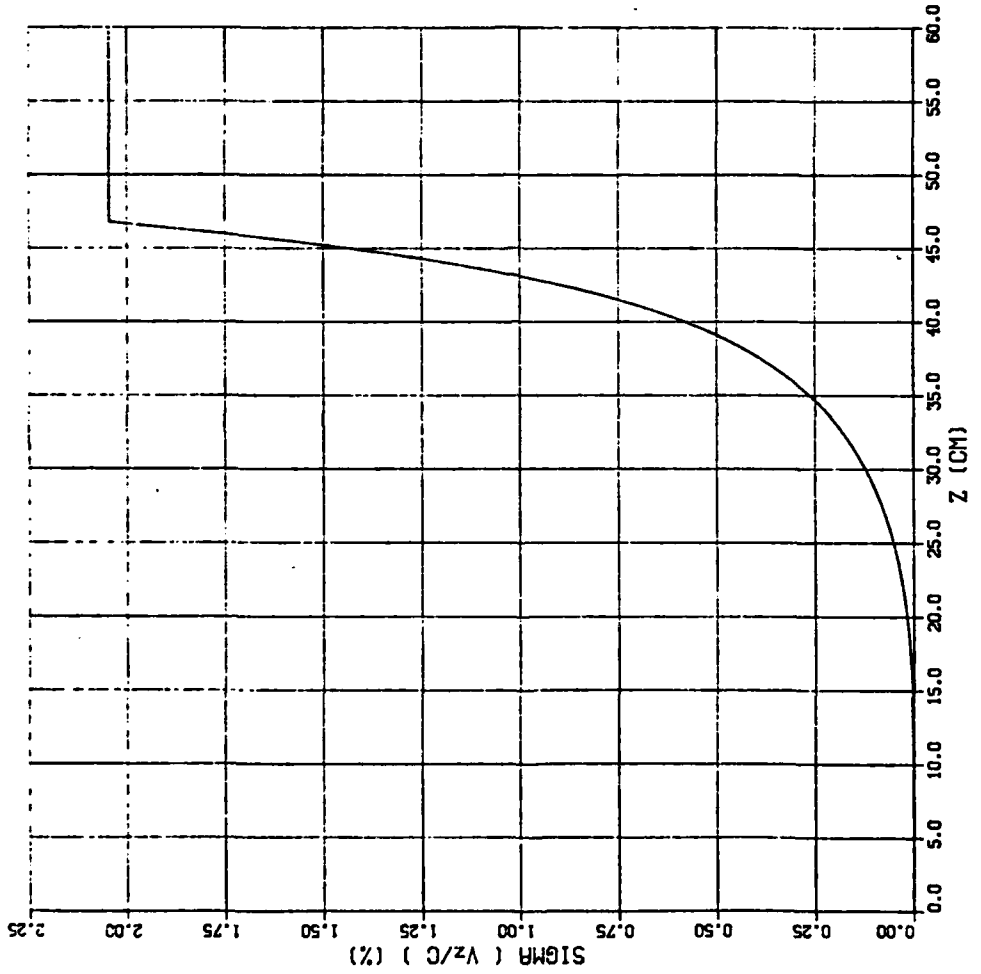

Figure 4-12 Standard deviation of the axial velocity in an adiabatic H-gun below resonance. B_z = 723 G, B_h = 31 G. (η = -0.135, ν = 0.037).

SECTION 5
DESIGN AND SCALING OF H-GUNS

The previous sections have developed the general characteristics of H-guns and how the various parameters interact. In this section the use of this information to design H-guns will be considered. Lacking a base of experimental results from which to draw, no final set of design rules can be established; however, with the general features developed in the previous sections, an outline for H-gun design can be given.

The theory which is applicable to the particular gyro-device being considered should provide the frequency, beam voltage, interaction α, and interaction guide field (B_2). Once these factors are established, then the interaction parameters are related to the helix exit parameters through conservation of energy and canonical angular momentum. At this point a choice must be made regarding either the magnetic field ratio or the α at the helix exit (α_h). Choosing either one determines the value of the other through the equation,

$$\alpha_h^2 = \frac{R\alpha^2}{1 + \alpha^2 - R\alpha^2} .$$

The α_h value determines the lines on the ideal H-gun curves (see Figures 2-4 and 2-6) which relate the fields and helix parameters. Then selection of n, ν, or the helix period determines the remaining values.

Having determined the helix parameters, one should now check to see if the criteria given in the earlier sections are satisfied. The H-gun should not be operating too close to gyroresonance and, if possible, should be operated above resonance. Also the period must be long enough to ensure that $r_{beam}/L \ll 1$. If the design passes these tests, then calculations should be done to determine the necessary helix field

magnitude. In general the required magnitude should be less than the ideal H-gun value, because the field increases off axis. Now one must determine if a helix can be designed to generate this field. Here, issues of wire size, coil cross section, and cooling must be considered. In the section on realistic helix fields recall that efficient field generation depended on keeping the helix radius small compared to the period. Also the nonadiabaticity of the exit (and entrance) depends on a small ratio. Taking these factors into consideration, a reasonable upper limit on the radius to design for is

$$k_w a \leq 2.$$

In addition we must also require

$$r_\perp < a$$

or

$$\alpha_h < k_w a \ .$$

This imposes a limit on the maximum helix period (or minimum radius) in order to prevent beam scraping. This limit should not be approached too closely in order to keep the beam a reasonable distance from the drift tube wall. One method for estimating the current required to produce the necessary field is to use the expression in Section 3 for the on-axis field magnitude with the helix radius set equal to the radius of the coil centroid and multiply by the number of wires in the coil. Thus,

$$I_h(\text{amps}) \approx \frac{B_h}{0.4 N_c a k_w^2 K_1'(k_w a)} \ , \quad a = r_{\text{centroid}}$$

N_c = # of wires in the coil.

If this current is consistent with wire size and cooling constraints, then a workable set of parameters has been determined. If not, then either the helix period must be changed to shift the H-gun closer to resonance, a smaller helix radius must be used, or a new magnetic ratio or exit α must be selected. An example using the parameters of Reference 1 is shown below.

Example

Interaction parameters:	$f \approx 5.2$ GHz
	$v_o \approx 65$ kV
	$B_2 \approx 1850$ G
	$\alpha \approx 1.5$
select $R \approx 1/2.5$:	$\alpha_h \approx .62$
	$B_1 \approx 740$ G
select $L \approx 6.67$ cm:	$B_T \approx 836$ G
	$\eta \approx -0.11$
	$\nu \approx 0.025$ adiabatic
	≈ 0.01 nonadiabatic

In Section 4 it was noted that if this H-gun had been operated above resonance, then the beam quality would have been improved. If the period had been lengthened to L = 7.54 cm, the H-gun would have operated above resonance; the compression ratio could have been changed to $R \approx 1/2.2$ to achieve the same result. Changing R would require a change in α_h from 0.62 to 0.68.

Once an H-gun design has been developed, tested, and found to be satisfactory, it can be scaled to other parameter domains by keeping certain normalized values and ratios fixed. Holding η and ν constant will keep the exit α_h constant. If the ratio of beam radius to helix period is also held constant, then the velocity spreads induced by the helix fields will be the same. For example, suppose that a shift in interaction frequency is desired, but the beam voltage is to remain constant. Set

$$\overline{f} = \lambda f,$$

then

$$\overline{B}_2 = \lambda B_2 \left(\overline{r}_{w.g.} = r_{w.g.}/\lambda\right)$$

$$\overline{R} = R$$

$$\overline{B}_T = \lambda B_T$$

$$\overline{L} = L/\lambda.$$

In order to leave η, ν, and α_h constant,

$$\bar{B}_l = \lambda B_l$$

and

$$\bar{B}_h = \lambda B_h \ .$$

Similar velocity spreads require

$$\bar{r}_{beam} = r_{beam}/\lambda$$

or

$$r_{beam}/L = \bar{r}_{beam}/\bar{L} = \text{constant} \ .$$

If the helix coils are scaled by $1/\lambda$, then the harmonic amplitudes are constant (see Section 3), and the helix field is automatically scaled if the helix current is the same. Scaling the helix coils in this manner can not be extended too far before the wire is unable to carry the current.

Thus, H-gun performance can be scaled by holding ν, η, r_{beam}/L, and a/L constant. Shifting to new parameters may require a new Pierce gun design in order to adjust the beam radius and keep beam ripple low. Two examples of scaling an H-gun design to higher frequencies are shown in Table 5-1. In each case the factors listed above are held constant, and, as can be seen, the performance characteristics are almost identical. Each of the helices listed in the table is buildable. The fabrication and necessary current-carrying capability would pose no problems for current technology.

TABLE 5-1
H-GUN SCALING

$k_w r_{beam} \simeq .31$, $k_w a \simeq 1.6$

	#1	#2	#3
scaling factor - λ	-	7	19
cyclotron frequency - GHz	5	35	95
beam voltage - kV	60	60	60
magnetic compression ratio	1/2	1/2	1/2
helix period - cm	6	0.85	0.31
helix current - amps	22	22	22
transition field - kG	0.89	6.26	16.98
η	0	0	0
ν	.05	.05	.05
computed α_h	0.87	0.88	0.86
computed $\sigma(\alpha_h)/\alpha_h$	2.4%	2.4%	2.6%

SECTION 6
CONCLUSIONS

The final question that must be addressed is whether the H-gun concept is a workable and competitive alternative to today's magnetron injection guns. In our opinion the results of the preceding sections clearly indicate that the H-gun can be at least competitive with MIGs and, in certain situations, may be clearly superior. Let us consider a few specific points:

Flexibility- The characteristics of the beam can be adjusted over a wide range of values by changing the bifilar helix or the Pierce gun, or both. Even with a fixed Pierce gun and helix, changes in voltage and axial field can be accommodated by adjusting the helix field. This is particularly true for adiabatic designs. H-gun flexibility is a clear plus for experimental research.

Beam Quality- Without space charge effects it appears possible to generate beams with $\alpha \simeq 1$ and axial velocity spreads $\Delta V_z/V_z < 2\%$ directly at the helix exit. Space-charge effects will increase the velocity spreads but probably not enough to make the H-gun worse than the MIG. At currents where the space charge is negligible, there should be very little degradation of velocity spread. The velocity spread can even be adjusted by changing the beam radius.

Beam Power- The H-gun can generate very high power beams with little or no modification, provided the beam radius is kept within reasonable limits.

Size- Here the MIG is superior, at least for modest electric fields in the gun region. The length required for beam formation and the helix will always make the H-gun larger.

Helix Field Requirements- The helical magnetic field does not have to be produced by electromagnetic coils. Both superconducting and permanent magnet designs are possible. These would reduce power requirements and could generate fields of several kilogauss.

Future H-gun research should include space charge effects and more realistic beam initial conditions. When possible, calculations should be extended to the interaction region. In addition, there are other configurations similar to the H-gun which might prove interesting. For example, there is no reason that the H-gun could not be operated with a hollow beam. Or, instead of a helical field, an oscillating linear or radial transverse field could be used to generate transverse velocity.

REFERENCES

1. P. Ferguson and R. Symons, IEDM Digest, 198 (1981).

2. K. Halback, Nuclear Instruments and Methods, Vol. 187(1), 109 (1981).

3. L. R. Elias and J. M. Madey, Rev. Sci. Instrum. 50 (11), 1335 (1979).

4. R. C. Wingerson, T. H. Dupree, and D. J. Rose, Phys. Fluids 7, 1475 (1964).

5. L. M. Lidsky, Phys. Fluids 7, 1484 (1964).

6. Ajit Singh and Ward D. Getty, IEEE Trans. on Electron Devies, Vol. ED-21, 93 (1974).

7. J. P. Blewett and R. Chasman, J. Appl. Phys. 48, 2692 (1977).

8. L. Friedland, Phys. Fluids 23, 2376 (1980).

9. P. Diament, Phys. Rev. A 23, 2537 (1981).

10. H. P. Freund and A. T. Drobot, Phys. Fluids 25, 736 (1982).

11. R. H. Jackson, S. H. Gold, R. K. Parker, H. P. Freund, P. C. Efthimion, V. L. Granatstein, M. Herndon, A. K. Kinkead, J. Kosakowski, and T. J. T. Kwan, J. Quantum Elec. special issue on free-electron lasers, March 1983.

12. R. H. Jackson, et al., BAPS 26, 909 (1981).

13. R. H. Jackson, et al., Abstracts of the 1982 IEEE International Conferenece on Plasma Science.

14. CRC Standard Math Tables

15. H. Poritsky, J. App. Phys. 30, 1828 (1959).

16. I. S. Gradshtezn and I. M. Ryzhik, Table of Integrals, Series and Products, (Academic, New York, 1980 4th edition). Sec 3.145.

17. Handbook of Mathematical Functions (eds. M. Abramowitz and I. A. Stegun, Dover, New York 1972), sections on Bessel functions and Struve functions.

18. Dr. P. E. Ferguson, private communications.

END

FILMED

10-84

DTIC